Strength of grass covers on dikes

Master thesis

by

C.J. Boon

TU Delft

INFRAM HYDREN
Hydraulic Engineering, Innovation & Research

Strength of grass covers on dikes

Master thesis

by

C.J. Boon

in partial fulfillment of the requirements for the degree of

Master of Science
in Civil Engineering

at the Delft University of Technology (TU Delft),
to be defended publicly on Wednesday January 19th, 2022 at 12:00 PM.

Student number:	4170539	
Project duration:	December 3, 2020 – January 19, 2022	
Thesis committee:	Dr. Ir. A. Antonini,	TU Delft, Section Coastal Engineering
	Prof. Dr. Ir. M.R.A. van Gent,	TU Delft, Section Coastal Engineering
	Dr. Ir. G.H. Keetels,	TU Delft, Department Marine & Offshore Technology Section Offshore & Dredging Engineering
	Ir. G.J. Steendam,	Infram Hydren
	Ir. R.J. Wegman,	Infram Hydren

An electronic version of this thesis is available at `http://repository.tudelft.nl/`.

Cover photo: Wave overtopping of a grass covered dike at Hartlepool, UK. Source: HR Wallingford.

TU Delft

INFRAM HYDREN
Hydraulic Engineering, Innovation & Research

In loving memory of

Xander Frederik Boon

Preface

Dear reader,

In front of you lies the final report of my master's thesis: Strength of grass covers on dikes. With this report, I will conclude my time as a student at the TU Delft. During these years, I learned an incredible amount of things, of which many are related to engineering. However, during these years I also learned a great deal about myself. This made my time as a student a fun, sometimes bumpy, although highly valuable experience.

I would like to dedicate this thesis to my brother Xander, who all of a sudden passed away last year. Dear Xander, I remember you for your kindness, your tranquility and your endless resilience. I thank you for all the beautiful moments we have shared together, for our strong bond and for your continuous support during my challenges. I miss you deeply and you will always be in my heart.

With these acknowledgements, I would like to thank everyone who have supported me and my family during our loss. Yet, I want to use these acknowledgements to thank everyone who made this thesis possible in these times.

First of all, I would like to thank my committee members for all their support during my thesis. From the TU Delft, I would like to thank Alessandro Antonini, Marcel van Gent and Geert Keetels for your insight and feedback. From Infram Hydren, I would like to thank Gosse Jan Steendam for your feedback and for the opportunity to participate in various measurement campaigns to acquire the necessary data. Furthermore, I would like to thank Rik Wegman for your guidance throughout my thesis, your knowledge on the topic and for your company and support during my measurements.

I also want to thank Gerben, Frans and the rest of the Grass on Sand team for the help they gave me and for all the fun moments at the dike while performing the experiments. Furthermore, I would like to thank Wetterskip Fryslan and Waterschap Drents Overijsselse Delta, for providing access to the various measurement locations.

Life does not only consist of work, and hence, I would like to thank my friends and fellow students for all the good times I have had during my studies and for your support during these times. It was always nice to be able to recharge my batteries by enjoying a beer or by doing an activity. These moments have helped me to keep my motivation to obtain this degree and for this, I wish you all the best in life.

And finally, I would like to thank my parents for all the support they gave me during my years at the TU Delft. Whatever the problem may be, I know I can always knock at your door, and for that, I thank you greatly. I hope for all three of us that we can leave these times behind and that we can live better days in the future.

C.J. Boon
Delft, January 2022

Abstract

Wave overtopping, in which a wave washes over the crest of a dike and damages its inner slope, is one of the many mechanisms that is found to be responsible for dike failures. As these dikes are generally covered with grass, insight into the erosion resistance of these grass covers against wave overtopping is desired. To assess the performance of dikes against wave overtopping, various concepts exist, such as the widely used cumulative overload method. However, these concepts lack a thorough understanding of the physical mechanisms at play during grass cover failure as a result of wave overtopping. Furthermore, the methods are generally not time-efficient and are labor intensive, leading to high costs. Therefore, a time-efficient and predictive method is desired that is based on the physical mechanisms of grass cover failure.

The grass pull device, which is used extensively in this thesis, may serve as an alternative for the existing assessment methods. The device, which is reminiscent of a tensile test used in mechanical sciences, is able to exert various load mechanisms on the grass cover. In this thesis, the grass pull device is used to study various aspects of grass cover failure. Special attention is given to the influence of cyclic loading on the grass cover. Additionally, material properties have been derived that may serve as input for numerical grass erosion models. Furthermore, the influence of grass roots, subsoil type and pore saturation on the failure mode of grass covers was investigated.

The results of this study showed a continuous growth of deformation and a decrease in stiffness when the grass cover is loaded cyclically. The behavior of grass during cyclic loading was found to be comparable to other composite materials, such as fiber-reinforced plastics. The material properties Young's and shear modulus were derived. The Young's moduli were found to be slightly overestimated, while the shear moduli were found to be comparable to what may be expected from literature. Differences in grass cover properties on different subsoils were identified, showing that grass covers on clay are generally better at resisting deformation, while having a brittle failure mode. For grass covers on sand, a large spread was observed and the material was found to deform easily, while still providing resistance at large deformations.

Based on the findings of this study, recommendations were made to improve the grass pull device. It was found that the grass pull device was successful in providing insight into various physical processes. Whether the grass pull device will be able to capture all relevant erosion mechanisms remains questionable, but it has proven to be a successful addition to existing assessment methods.

Contents

List of Figures

List of Tables

1 Introduction

1.1. Background

Flooding of land is a major risk in low lying areas. The impact of flooding can be quite severe, ranging from substantial infrastructural and economical damage to loss of life in extreme cases. To counter flooding, low lying areas are often protected by earthen dikes. However, under stormy conditions, these dikes may be loaded heavily by the combination of waves, tides and surges, which may cause dike failure. Several mechanisms can be held responsible for dike failure. Among these mechanisms is the process of wave overtopping, in which a wave washes over the crest and the landward slope of the dike, causing erosion to the protective grass layer. Wave overtopping has been thought to be responsible for dike failures during the North Sea flood of 1953 and the 2004 flood caused by hurricane Katrina around New Orleans.

To reduce the risk of flooding to a minimum, it is important that the assessment criteria for the performance of dikes remain up to standard. In 2017, a new criterion was adopted by the Dutch government to assess the resistance of the Dutch dikes against flooding. This criterion is called the Wettelijk Beoordelingsinstrumentarium 2017 (or WBI2017) and it is intended for the Dutch water boards to assess whether the dikes under their management comply to the standards. Usually the Dutch dikes had to withstand a certain water level in order to be considered as safe. However, as of 2017, the dikes are assessed in a different way; not only the exceedance of a certain water level in combination with wave action has to be taken into account in the assessment, but also the consequences of flooding. Hence, dikes will be assessed based on a flood risk approach. In order to assess dikes with this criterion, more insight is required in the many possible failure mechanisms of these dikes under various types of hydraulic loads. Since dikes in the Netherlands are generally covered with grass, part of the WBI2017-criterion focuses on the failure of a grass cover under hydraulic loads (De Waal, 2016). It gives several calculation rules to assess the strength of grass covers for dikes. However, knowledge of the exact failure mechanisms of grass covers is limited and therefore it is desired to have a better understanding of these processes.

One of the failure mechanisms listed in the WBI2017-criterion that requires a better understanding is the previously mentioned phenomenon of a grass cover eroding due to overtopping waves. It is a challenging topic since various processes and failure mechanisms play a role, of which some have not yet been identified. Furthermore, the grass cover is an anisotropic material, having its properties varying significantly on a spatial scale. Additionally, the hydraulic load caused by an overtopping wave is very variable in nature as a result of turbulence, which makes it difficult to determine how the load interacts with the grass cover.

Over the years, much research has been carried out to get an indication of the erosion resistance of a grass cover during wave overtopping. From various experiments (Steendam et al., 2009, 2012, 2014; Van der Meer et al., 2009a), it was found that the grass cover does not fail after only one overtopping event, but rather due to the cumulative damaging effect of many consecutive overtopping events. Hence, fatigue plays a role with regard to the onset of failure of the grass cover. To quantify and predict this cumulative damaging effect of overtopping waves, Van der Meer et al. (2010) derived the cumulative overload method. This method assesses the cumulative damage that overtopping waves cause on a grass slope by means of a velocity threshold, or

more specifically, a critical velocity. Other grass erosion models exist as well, such as the method of Dean et al. (2010), Hughes (2011) and Hoffmans (2012). Furthermore, to gain additional insight into the fundamental processes and prediction of grass cover failure, several numerical models have been developed over the years. These numerical approaches are based on various principles, such as the development of soil stresses (Mersie, 2021; Van Langevelde, 2018) or the exceedance of a shear stress threshold (van Bergeijk et al., 2019a; Van Bergeijk, 2018; van Bergeijk et al., 2019b). All previously mentioned approaches are covered in more detail in Chapter 2.

As grass is a material that is difficult to scale down properly (Van der Meer et al., 2007), full scale experiments are the best option to validate these theoretical models. Van der Meer et al. (2007) developed a wave overtopping simulator to simulate overtopping events at real dikes, which is shown in Figure 1.1a. Since its development, many tests have been performed to assess the cumulative overload method with this simulator (Steendam et al., 2009, 2012, 2014; Van der Meer et al., 2009a). The cumulative overload method in combination with the wave overtopping simulator has predictive value. However, the method has its drawbacks. Whereas failure of the grass cover can be relatively well described by the method (Steendam et al., 2012), the criteria for start of damage and damage occurring at multiple spots are less well defined (Hoffmans et al., 2018; Van der Meer et al., 2015). Furthermore, the method does not highlight the mechanical processes occurring in the grass cover during failure (Wegman, 2020). With regards to the practicalities of the method, the wave overtopping simulator tests require a significant time to prepare, since the simulator has to be brought to the dike with a truck and has to be installed with a crane. Additionally, a wave overtopping simulation can take up to approximately 6 hours, since the overtopping simulator requires a certain time to simulate the various water levels and wave conditions associated with the peak of a storm. For these reasons, it may be desirable to have access to a test that is able to quickly assess the strength of a grass cover, which is based on more fundamental mechanical properties of the grass cover.

A more practical device for assessing the erosion resistance of the grass cover is the grass pull device, which is shown in Figure 1.1b. It has been developed to measure the tensile strength of the grass cover. With the device, various tests are possible to test the behavior of grass covers under different loading conditions. The grass pull device can be easily operated, is easily transportable and is time efficient, such that many grass pull tests can be performed to test the variability of the grass cover strength. Several studies have been performed with the grass pull device to investigate its applicability in assessing the grass cover strength during wave overtopping. Bijlard (2015) used the device to determine the normal tensile strength of an intact grass sod. A practical method was developed in which these results were combined with a formulation by Hoffmans (2012) to determine the critical velocity. The results for the critical velocity determined with the grass pull tests were compared with critical velocities found with the overtopping simulator, resulting in a reasonable agreement between the two methods. Wegman (2020) used the grass pull device to further investigate several strength properties, such as the influence of cohesion, the grass roots and fatigue. Damage accumulation was found to occur during cyclic loading of the grass cover, with its stiffness decreasing over time.

(a) Wave overtopping simulator. Adapted from: Van der Meer et al. (2009b)

(b) Grass pull device

Figure 1.1: Various grass cover assessment methods.

The results by Bijlard (2015) and Wegman (2020) have proven that the grass pull device is able to reveal new insights regarding grass cover failure and that the device may have predictive value. However, several mechanical processes that occur during grass cover failure are still not identified. Since the grass pull device is continuously being developed, with its most recent and notable adjustment the transition from a manually operated device to an electronically operated device, more accurate results are expected to be generated by the device. Therefore, the possibility arises to further investigate the various physical processes of grass cover failure and to re-evaluate some of the concepts from previous work.

1.2. Objective and framework

For this thesis, the grass pull device is used to further investigate several of the physical characteristics of a grass cover, with the aim to get a better understanding of what parameters determine the grass cover strength. As was previously mentioned, fatigue was found to play a role in the failure of a grass cover during wave overtopping, as failure is often observed after many consecutive waves exceed a certain erosion threshold. From the literature review, the insight into the fatigue of a grass cover was still found to be limited. Furthermore, to improve the predictive value of the grass pull device, it is desired to quantify the strength reduction induced by fatigue.

Additionally, for the application and development of numerical models to simulate grass cover failure, such as the soil stress-based approaches by Van Langevelde (2018) and Mersie (2021), certain input parameters are required, such as the Young's modulus and the shear modulus. These parameters are usually well known for soils, however, literature provides little insight into these parameters for grass covers.

The interaction between soil and roots is generally thought to be the cause of the erosion resistance of grass covers (Muijs, 1999). However, what failure mechanisms of the soil-root system occur exactly during grass cover failure are not clear. These mechanisms may very well differ for subsoils with different characteristics, such as sand or clay. Hence, additional insight is desired.

During the winter of 2020-2021, several measurement campaigns have been held to assess the strength of grass covers at several locations in the Netherlands and Belgium. For this thesis, it was possible to partake in these projects and to do additional measurements. The first measurement campaign is the Grass on Sand project, which aims at assessing the strength of the grass cover of the sandy Vechtdijk between Zwolle and Dalfsen. Wave overtopping and wave impact tests have been executed at several locations, as well as grass pull tests, spread out over a time span of approximately 7 weeks. The second project is the POV Waddenzeedijken-project, a measurement campaign which is held to assess the grass cover strength of four dike stretches along the Wadden Sea. An additional small measurement campaign was held during the Polder2C's-project along the sea dike of the Hedwige-Prosperpolder. For this thesis, the main campaigns of interest were the campaigns at the Vechtdijk and the Waddenzeedijk, since the differences in failure characteristics between a sandy dike (Vechtdijk) and a clayey dike (Waddenzeedijk) could be investigated. Hence, grass pull tests have been executed at two locations along the Vechtdijk, located near the town of Dalfsen. The tests on the clay dike have been executed on the Waddenzeedijk, near the village of Oosterbierum. Furthermore, a small amount of measurements have been performed at the sea dike of the Hedwige-Prosperpolder.

1.3. Research questions

The desire for a better predictive method for grass erosion during wave overtopping, as well as the desire to have a better understanding of the processes involved during grass cover failure, leads to the main research question of this thesis:

How can the grass pull device be used to gain insight into the mechanical properties and processes of grass cover failure during wave overtopping?

To answer this research question, the following sub-questions are desired to be answered:

- What are typical values for the Young's modulus and shear modulus for a grass cover? How is the grass pull test able to quantify these parameters?
- How do pore saturation, grass roots and subsoil type influence the failure mode of a grass cover?
- What is the influence of repeated loading on the tensile strength of a grass cover and how can this effect be quantified?

1.4. Thesis outline

This report treats the main findings of this research. For this research, a literature review has been performed, which formed the basis for the design of several field experiments. The results from these tests have been analysed and have been reflected upon by relating them to existing work. After this review, the main conclusions for the thesis have been noted and recommendations for future research have been made. Based on these various research steps, an outline for the various thesis chapters is generated, which is listed below:

1. **Introduction:** Introduces the main topic to the reader. Provides the background and the framework in which the thesis takes place. Also highlights the knowledge gap that was found during the literature study. Based on this knowledge gap, research questions are formulated that will serve as main objectives for this thesis.
2. **Theory:** Lists the theoretical framework in which the thesis will be set. The state of the art knowledge will be elaborated, which will serve as a tool for subsequent chapters.
3. **Methods:** Elaborates on the methods that are required to reach the thesis objectives. In this chapter the required tools and types of tests are described. Also a description will be given on how the analysis of the test results is executed.
4. **Results:** Describes the results of the various tests and analyses.
5. **Discussion:** Discusses the obtained results. In this chapter the results are critically reviewed for correctness. Processes that may have influenced the results are identified and reflected upon.
6. **Conclusions:** assesses whether or not the research objective is reached. The research questions are answered based on the results from the various tests and analyses.
7. **Recommendations:** Aims at recommending further research steps based on the discussion and the conclusion.

2

Theory

In this chapter, the theory related to the erosion of grass loaded by overtopping waves will be elaborated. As the thesis will be mainly focussed on the physical characteristics that determine the strength of grass covers, wave overtopping is briefly reflected upon, as is done in Section 2.1. In Section 2.2, a basic description of a grass cover is given. To asses the quality of these grass covers, several classification methods exist, which are treated in Section 2.3. The mechanical properties of grass covers are treated in Section 2.4. The grass cover strength and the characteristics of wave overtopping are linked together in several erosion models and is treated in Section 2.5. Numerical approaches for grass cover erosion are found in Section 2.6. Finally, a summary of the most important concepts from the literature review is given in Section 2.7.

2.1. Wave overtopping

The process of wave overtopping consists of various steps, which are illustrated in Figure 2.1. The process starts with a wave breaking on the outer slope of a dike. As a result of its horizontal velocity, the broken wave runs up towards the crest of the dike. During this run up period, the wave is negatively influenced by both gravity and friction, which causes the flow to slow down and decrease in size. Before reaching the crest, part of the water running up will run down the outer slope. Once the flow reaches the crest, it is further influenced by friction, causing both flow velocity and thickness of the wave to decrease. Upon reaching the landward slope, the flow may separate as a result of the high flow velocity on the crest. When flowing down the landward slope, the flow is accelerated by gravity. However, friction slows the flow down, which in the end will result in a constant flow over the dike that is balanced by friction and gravity.

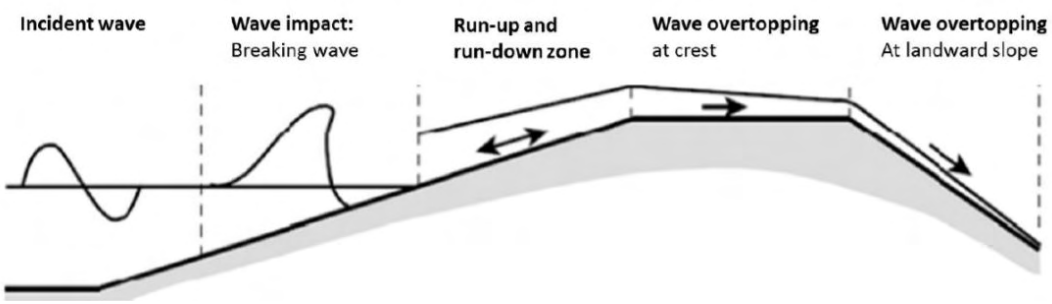

Figure 2.1: Various stages in the development of an overtopping wave. From: Schüttrumpf and Oumeraci (2005)

The most important characteristics of wave overtopping that are relevant for grass erosion are listed in this chapter. Additional information on the physics of wave overtopping is given in Appendix A.

2.1.1. Load mechanisms by overtopping waves

Several load mechanisms are responsible for grass erosion during wave overtopping. Van Langevelde (2018) mentions three main load mechanisms to be exerted on the inner slope of the dike. One of these mechanisms is the generation of a shear stress that is imposed on the grass cover. When sufficiently strong, the shear stress is balanced by the resistance of the grass cover. However, the roughness of the grass cover causes eddies to develop in the water, leading to turbulence in the overtopping wave. The occurrence of turbulence is the second load mechanism, which is paired with the observation of fast pressure fluctuations, which can either be positive or negative. These turbulent pressure fluctuations can cause lift forces to be exerted on the grass cover Hoffmans et al. (2009). Other load mechanisms that play a role in the erosion of grass covers is the occurrence of jets. These hydraulic loads are often observed at transitions of the dike geometry, for instance between the crest and the landward slope (Ponsioen, 2016; van Damme et al., 2016) or at the toe of the dike Valk (2009). The erosion mechanisms that play a role during jets may be described by the breach initiation process (Ponsioen, 2016).

2.1.2. Turbulence

As explained in Section 2.1.1, the flow in overtopping waves is highly turbulent, in which air entrainment often occurs. However, insight in turbulence is limited and is therefore one of the main problems encountered when formulating a physically based erosion criterion. Turbulence is often described by the relative turbulence intensity r_0, which can be determined in various ways. The concepts are summarized by Hoffmans (2012):

$$r_0 = \frac{\sqrt{k_0}}{U_0} = \frac{\sqrt{\frac{1}{h}\int_0^h \frac{1}{2}\left(u_{RMS}^2 + v_{RMS}^2 + w_{RMS}^2\right)}}{U_0} = \alpha_0 \frac{u_*}{U_0} = \alpha_0 \frac{\sqrt{g}}{C} \tag{2.1}$$

In these relations, U_0 is the mean flow velocity. k_0 is the depth-averaged turbulent energy, which is determined with the root mean square of the turbulent fluctuations in the three main directions (u_{RMS}^2, v_{RMS}^2 and w_{RMS}^2). α_0 is a coefficient with the value of 1.2 and u_* and C are the shear velocity and the Chézy coefficient respectively. The relative turbulence intensity can be related to the bed shear stress by:

$$\tau_0 = \alpha_0^{-2} \rho (r_0 U_0)^2 \tag{2.2}$$

The maximum pressure fluctuation by turbulent motion can be described by:

$$p_m = \alpha_\tau \tau_0 \tag{2.3}$$

In which α_τ is a coefficient with the value of 18. Using Equation 2.2, the maximum pressure fluctuation can also be determined by:

$$p_m = \alpha_\tau \alpha_0^{-2} \rho (r_0 U_0)^2 \tag{2.4}$$

The maximum pressure fluctuation may cause uplift forces to be exerted on the inner dike slope (Hoffmans et al., 2009), possibly causing failure of the grass cover. An erosion model in which the maximum pressure fluctuation is incorporated is the Turf Element Model as proposed by Hoffmans (2012). This model is treated in Section 2.5.1.

2.1.3. Failure mechanisms

As was observed from Section 2.1.1, overtopping waves impose various load mechanisms on the dike, which in turn causes different failure mechanisms to be observed. The report Handleiding Dijkbekledingen Deel 5: Grasbekledingen (Van der Meer et al., 2015) mentions several failure mechanisms that are observed during tests with the wave overtopping simulator. Several of the described failure mechanisms are displayed in Figure 2.2. The mechanisms that are often observed are:

- **Pull out mechanism**
  This mechanism can be described as a grass sod of about 15 by 15 cm that suddenly disappears from the cover layer. Due to the highly turbulent fluxes as a result of the overtopping wave, an under pressure is generated above the cover layer. This causes an imbalance in the vertical force equilibrium for the grass sod which in turn can lead to pulling out of the grass sod.

- **Wear erosion**
  As the name suggests, this mechanism causes slow erosion as a result of the entrainment of matter by the overtopping wave. This mechanism is observed for not fully covered grass covers or for sandy, low cohesive top layers. Although this mechanism was observed during overtopping simulator tests, it was not found to be the normative erosion mechanism for failure of the grass cover.

- **Jet erosion**
  Jet erosion is a mechanism that mainly occurs at transitions from a dike slope cover to a horizontal toe. The water running down the slope will form a jet on the horizontal part of the dike, as a result of the rapid change in flow direction. This concentrated flow on the horizontal layer may cause erosion of the cover. Often it is found that a scour hole develops at the toe of the dike as a result of this mechanism.

- **Peel erosion**
  When the cover layer is already damaged somehow, then the downstream cover layer will be exposed to the overtopping flow. As a result of this, peel erosion may occur, in which the downstream cover layer will slowly be stripped from the underlying layers, leading to long stretches of eroded cover downstream.

- **Head cut erosion**
  Head cut erosion occurs when several of the aforementioned mechanisms act together. When a hole starts to develop as a result of pull out or peel erosion, it may happen that due to cumulative overtopping the sandy dike core becomes exposed as a result of wear erosion. Since sand has no cohesion, it's more easily eroded. This causes geotechnical instability of the dike, since the vertical sandy walls in the hole will slide as sand is not cohesive. As a result of this, the hole may expand in the upward slope, causing failure of the cover layer lying on top.

(a) Pull out erosion

(b) Jet erosion at the toe of the dike

(c) Peel erosion

(d) Head cut erosion

Figure 2.2: Various erosion mechanisms that may occur during wave overtopping. From: Van der Meer et al. (2015)

From Section 2.1.1, it was observed that turbulence causes pressure fluctuations, causing either pressure or uplift forces to be exerted on the grass cover. These uplift forces may cause initiation of the pull out mechanism, which is often found to be occurring at the start of several other erosion mechanisms (Van der Meer et al., 2015). The maximum pressure fluctuation p_m, as found in Section 2.1.2, may therefore be a desirable design load. The pull out mechanism is simulated with the grass pull device, which emulates the lift force caused by pressure fluctuations. This is done by imposing a tensile force on the grass cover.

2.2. Basic description of a grass cover

Grass covers are very variable in nature. Grass is an anisotropic material, which means its properties are varying in the different directions. Its roots are varying in length and are extending into the soil over various heights. Additionally, there is the presence of all kinds of vegetation. A grass cover does not merely consist of multiple grass types, but also of different types of weeds, plants or mosses. The composition of the grass will depend on dike orientation, amount of soil moisture and competition between species. Also the presence of wildlife on a dike, such as moles, mice, worms and insects affect the composition of the grass cover.

The report Handreiking Dijkbekledingen Deel 5: Grasbekledingen by Van der Meer et al. (2015) describes different elements of a grass cover as displayed in Figure 2.3. Above the top layer, the grass cover consists of the leaves of the vegetation, which is called the sward and the stubble, which is the part of the vegetation that remains when the cover is mowed. The topsoil is the part of the cover where the most roots are present, along with sand and clay particles. It generally has a thickness of approximately 0.2 m. The most densily rooted part of the topsoil together with the stubble forms the turf. Compared to the underlying layers it is porous and behaves elastic in moist conditions (Muijs, 1999). The amount of roots decrease with depth. The layer under the topsoil is called the subsoil, a layer in which hardly any roots are present. It consist mainly of a mix

of clay and sand and is generally not very permeable.

As described in Van der Meer et al. (2015), the root structure of a grass cover can generally be divided in three parts, of which two are located in the topsoil.

1. A zone with a closely packed root structure, which extents from the surface to about 5 cm depth, which is commonly referenced to as the sod. This structure usually develops in a year after the first installment of the grass cover.
2. A zone in which firm roots are present with a density of about 3 - 10 roots / dm^2. This zone usually extents to 0.2 - 0.4 m beneath the surface. Normally, this layer is largely developed after 1 - 2 years after first installment of the grass cover.
3. A zone with a root density of about 0.5 - 2 roots / dm^2. This zone can extent 1 m into the soil layer.

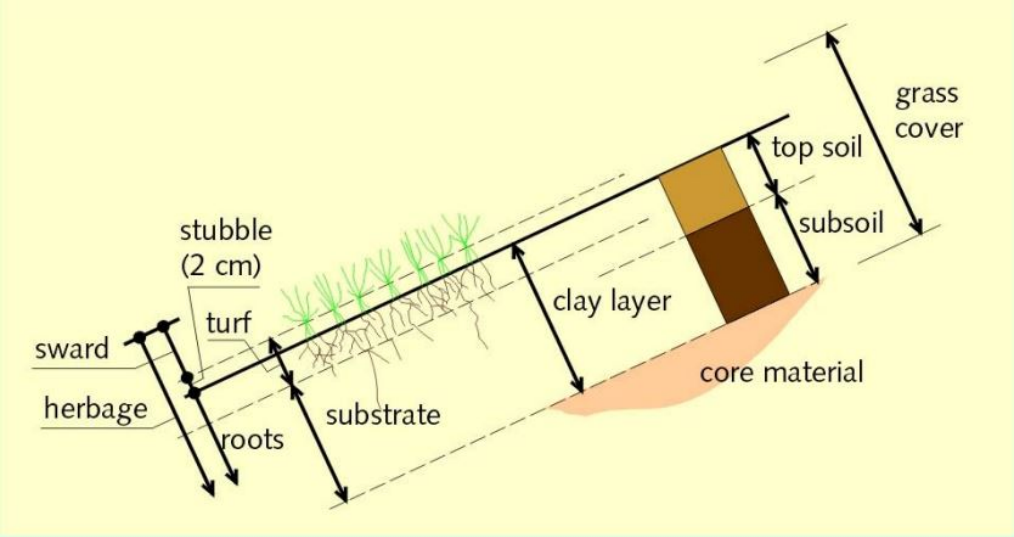

Figure 2.3: Basic description of a grass cover. From: Muijs (1999)

As stated at the start of this chapter, many different biological processes take place in a grass cover. As a result of these processes, a particular soil structure is formed in the cover, which is constantly changing over time. Due to the growth of grass roots (as well as due to other biological activity), micro cracks are being formed in the soil, forming lumps of soil that are called aggregates. Deposited minerals and sticky biological substances that are excreted by the grass roots causes cementation of the soil particles and the aggregates, effectively binding them together. Figure 2.4 displays the soil structure for a grass cover. It shows that the aggregate size is small in the top part of the grass sod, as a result of the high root density. When travelling deeper into the soil, the root density decreases and as a result, the aggregate size increases.

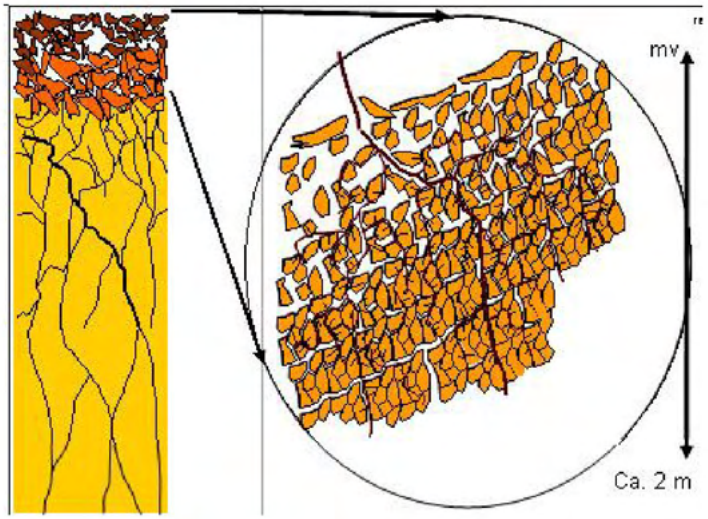

Figure 2.4: Soil structure in a grass cover. From: Van der Meer et al. (2015)

2.3. Classification of grass covers

Grass covers are often classified based on their quality, as the quality varies significantly over various locations. An assessment based on the quality of a grass cover is important, as it tells something about its erosion resistance. The grass cover quality can generally be defined in three different ways, namely by maintenance type, by ecological measurements and by root counts. These are covered in Sections 2.3.1, 2.3.2 and 2.3.3 respectively. The three methods are described in VTV2006 (Ministerie van Verkeer en Waterstaat, 2007).

2.3.1. Maintenance type

Most of the time, grass is classified based on maintenance type. The maintenance types can be distinguished by the following four categories:

A For this maintenance type the grass cover is being hayed and/or grazed by sheep. In the case of haying, the resulting hay will be removed from the grass cover. Fertilization of the grass cover will not be done for this maintenance type. This maintenance type results in a good erosion-resistant grass cover.

B For this maintenance type more extensive grazing will be done, as well as light fertilization. This maintenance type results in a reasonable erosion-resistant grass cover.

C This maintenance type is characterised by heavy fertilization, as well as intensive grazing. This maintenance type results in a poor erosion-resistant grass cover. This implies that the erosion resistance of the cover for this maintenance type is largely governed by the soil in and under the grass sod.

D This maintenance type is characterised by over-fertilization, very intensive grazing by sheep, grazing by cattle or flail mowing without hay removal. This maintenance type results in a very poor erosion-resistant grass cover and thus, the maintenance type is highly unsuitable for maintaining dike covers.

When dealing with dike slopes faced to the north, substantial moss growth can occur, which makes the assessment based on maintenance type unsuitable. In these cases, an assessment based on root counts is more suitable.

2.3.2. Vegetation type

In case the maintenance type of the dike is unclear, a quality assessment can be based on the ecology of the grass cover. Based on the types of species present in the grass cover, a first estimate of the grass strength can be done, since the types of species encountered in the cover is strongly correlated to the type of maintenance. Using this information, again the maintenance type can be used to get preliminary estimation of the grass cover's erosion resistance. This preliminary estimation can be further verified by determining the percentage of cover over the dike and by determining the amount of roots.

In Table 2.1, the vegetation types are listed, along with the corresponding maintenance type and the sod quality. Also the amount of coverage and the root density are displayed for informative purposes. For the coverage, some additional requirements hold, which are given as:

- For M2 and H2 it holds that:
  - When the coverage is more than 70%, the sod quality is 'Reasonable'.
  - When the coverage is less than 70%, the sod quality is 'Poor'.
- For M3 and H3 it holds that:
  - When the coverage is more than 70%, the sod quality is 'Good'.
  - When the coverage is less than 70%, the sod quality is 'Poor'.

Table 2.1: Classification by vegetation type. From: VTV2006, Bijlard (2015)

Vegetation type	**Maintenance type**	**Coverage**	**Root density**	**Sod quality**
P: Pioneer vegetation with low species diversity	D	Reasonable / Poor	Poor	Poor
M1: meadow-grass / ryegrass	D/C	Good	Poor	Poor
M2: Meadow with moderate species diversity	B	Good	Poor	Poor
M3: Meadow with high species diversity	A	Reasonable	Good	Good
R: Rough hayland	D	Very poor, many open spots	Poor, heterogeneous	Poor
H1: Hayland with low species diversity (or fertilization)	D	Poor	Poor	Poor
H2: Species moderate Hayland	B	Reasonable	Reasonable	Reasonable
H3: Species rich hayland	A	Reasonable	Good	Good

2.3.3. Root counts

When classification based on maintenance type or vegetation type could not be performed, root counts may be performed. For this, on four locations in an area of 5 x 5 m, a gouge of with a diameter of 3 cm is put into the ground to extract soil samples. The upper 20 cm of the sample will be cut with a knife into parts of 2.5 cm. In these 2.5 cm parts, the amount of roots will be counted, where it is important that these are at least 1 cm long to be classified as roots. The amount of roots per slice should be listed such that a profile is obtained with the amount of roots over the depth. Such a profile can than be compared with the diagram of Figure 2.5. In this diagram, the profile is shown by the dashed line. The four coloured areas mark the different qualities of the grass cover.

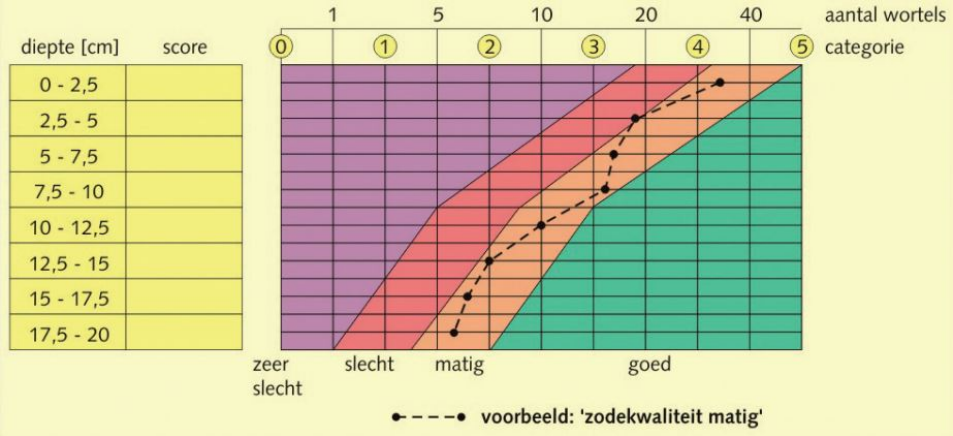

Figure 2.5: Classification of the grass sod based on root counts. From: VTV2006

Generally, the points of the profile will be located in the same area. However, if a minimum of two points are not located in the same area, the lowest classification is normative in determining the grass cover quality.

2.4. Mechanical properties of grass covers

2.4.1. Grass strength

The roots of the grass combined with the soil structure provides significant erosion resistance. It is often found that after erosion of the topsoil, the cemented and root-reinforced subsoil is still very resistant against erosion (Van der Meer et al., 2015). For the development of a physically based method to assess the strength of a grass cover, insight into the various grass cover characteristics is required.

The failure mode of grass roots is largely determined by the characteristics of the roots, the soil and its moisture content (Pollen, 2007). Roots in the grass cover may either be pulled out of the soil or may break. The percentage of roots failing due to one of these mechanisms is determined by a combination of these grass cover characteristics.

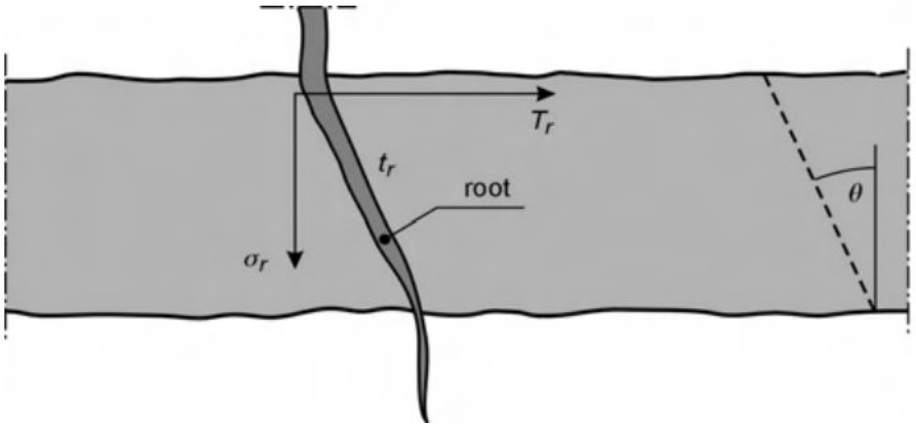

Figure 2.6: Definition of root stresses. From: Hoffmans (2012)

To determine the strength of grass sods, Hoffmans et al. (2009) expanded the Mohr-Coulomb criterion for soil with the root cohesion. The criterion can now be presented as:

$$\tau_s = c_e \cos\phi_e + c_r + (\sigma - p_w) \sin\phi_e \tag{2.5}$$

In this relation, τ_s is the shear strength, c_e is the effective soil cohesion, ϕ_e is the effective internal friction angle, c_r is the root cohesion, σ is the soil normal stress and p_w the pore water pressure. To determine the root cohesion, the following formula by Wu et al. (1979) is often used:

$$c_r = \frac{A_{root}}{A_1}(\sigma_{root,v}\tan\phi + \sigma_{root,h}) = \sigma_{root}\frac{A_{root}}{A_1}(\cos\theta\tan\phi + \sin\theta) \tag{2.6}$$

In which, $\sigma_{root,v}$ and $\sigma_{root,h}$ are both the vertical and horizontal component of the root stress respectively. The fracture A_{root}/A_1 is called the root area ratio (RAR), a measure for the total cross sectional area of the amount of roots over a standardised area of 1 m^2.

Based on the work of Sprangers (1999), Hoffmans (2012) found a relation for the critical mean grass normal strength, distributed over the depth:

$$\sigma_{grass,c}(z) = \sigma_{grass,c}(0)e^{\frac{z}{\lambda_{ref}}} \tag{2.7}$$

With:

$$\sigma_{grass,c}(0) = \frac{A_{root}(0)}{A_1}\sigma_{root,c} \tag{2.8}$$

In these equations, $\sigma_{grass,c}(0)$ is the critical mean grass normal stress near the surface, λ_{ref} is a reference height that ranges between 5 - 10 cm and $\sigma_{grass,c}(z)$ is the critical mean grass normal stress at any level. z is the depth which is defined negative when moving into the soil. The factor $A_{root}(0)/A_1$ is the RAR near the surface.

Bijlard (2015) used the grass pull test to derive a practical method to determine the critical grass mean normal stress, which is given by the following equation:

$$\sigma_{grass,c} = \frac{\alpha[F_4 + (F_2 - F_4)]}{A_b + 4\cdot A_s} \tag{2.9}$$

In this equation, F_4 is the force required to pull out a sod with 4 sides of the sod cut loose and F_2 is the force required to pull out a sod with 2 sides cut loose. α is a shape factor accounting for the contribution of the corners to the development of the failure plane, which has a value of 1.10 for the 20 x 20 cm^2 pull frame. A_b and A_s represent the area of the horizontal failure plane and the four side planes respectively.

Bijlard also compared the practical method with a rewritten form of the method by Hoffmans. It was found that the practical method provided a more accurate estimate, but the assumptions made by Bijlard to rewrite Hoffmans' method may have influenced this result.

2.4.2. Soil mechanics

The main soil types found in the grass covers of dutch dikes are either sand or clay. Both are porous granular materials, in which the pores may be filled by either gasses (air) or liquids (water). The strength of the material comes from the contact forces between the soil grains, however, the medium in the pores may reduce these forces as a result of buoyancy. A measure for the stresses induced by these contact forces is found by Terzaghi and Peck (1948), which is called the effective stress principle. In this principle, the total stresses in the soil are related as the sum of the pore pressure and the effective stresses (Verruijt, 2001), or more specifically:

$$\sigma = \sigma' + p \tag{2.10}$$

With σ the total stress, σ' the effective stress and p the pore pressure. Since the effective stresses are a measure of the granular contact forces in the soil, they are of importance for determining the strength parameters of the material. For soil, several of these strength parameters are listed below (Winterwerp and Van Kesteren, 2004):

$$E = \frac{\Delta\sigma}{\Delta\epsilon} \tag{2.11}$$

$$G = \frac{\Delta\tau}{\Delta\gamma} \tag{2.12}$$

The two parameters may be related to each other by (Verruijt, 2001):

$$G = \frac{E}{2(1+\nu)} \tag{2.13}$$

In which ν is the Poisson ratio.

Water is able to flow through the soil skeleton. For laminar flow in the soil skeleton, which is often the case due to soils having a relatively low conductivity, Darcy's law is the relation describing the flow of water in the pores of the soil. The relation is given as:

$$q = k\frac{\partial h}{\partial z} \tag{2.14}$$

A low hydraulic conductivity hinders the water to flow out of a soil volume loaded by compression. Soils such as clay typically have low conductivities as a result of the small tightly packed particles and small pores in between them. When these soils are loaded, the drainage of the water is hindered by the low conductivity, which causes an increase of the water pressure in the soil which takes a long time to dissipate. This process retards the deformation of the soil and is called consolidation. The consolidation problem is a diffusion process of the water pressure, which can be described by the following differential equation:

$$\frac{\partial p}{\partial t} = c_v \frac{\partial^2 p}{\partial z^2} \tag{2.15}$$

In which c_v is the consolidation coefficient, which is given by:

$$c_v = \frac{k_s}{\gamma_w(m_v + n\beta)} \tag{2.16}$$

In which n is the porosity and β is a measure for the compressibility of water. Since the compressibility of water is almost zero, this value can be omitted, which reduces Equation 2.16 to:

$$c_v = \frac{k_s}{\gamma_w\left(\frac{1}{K+\frac{4}{3}G}\right)} = \frac{k_s}{\gamma_w(\frac{1}{E})} \tag{2.17}$$

An analytical solution for the problem described in Equation 2.15 is given by the following equation:

$$U = 1 - \frac{8}{\pi^2}\sum_{j=1}^{\infty}\frac{1}{(2j-1)^2}\exp\left[-(2j-1)^2\frac{\pi^2}{4}\frac{c_v t}{h^2}\right] \tag{2.18}$$

In which U is the degree of consolidation, a quantity that quantifies how far the consolidation has progressed. It is defined as:

$$U = \frac{\Delta h - \Delta h_0}{\Delta h_\infty - \Delta h_0} \tag{2.19}$$

In which Δh is the strain at the moment of measurement, Δh_0 is the strain just after the start of loading of the soil and Δh_∞ is the strain when all the excess water pressure have dissipated.

2.4.3. Suction pressure and infiltration

In Section 2.2, it was described that the cover layer of a dike generally consists of structured soil made of clay or sand aggregates, with roots in between. Due to the small pores between these aggregates, water is able to be sucked into the pores as a result of capillary forces. These negative pore pressures cause strengthening of the grass cover, leading to a higher resistance against erosion.

During wave overtopping or precipitation, water will infiltrate into the grass cover. The water will percolate into the large pores between the aggregates, causing a decrease of these capillary pressures and leading to a weakening of the soil. However, since the aggregates itself often have a low permeability, it takes time for the suction pressures inside the aggregates to dissipate. Hence, the pore pressures inside the aggregates may stay negative while the pore pressure between the aggregates is positive. This is illustrated in Figure 2.7.

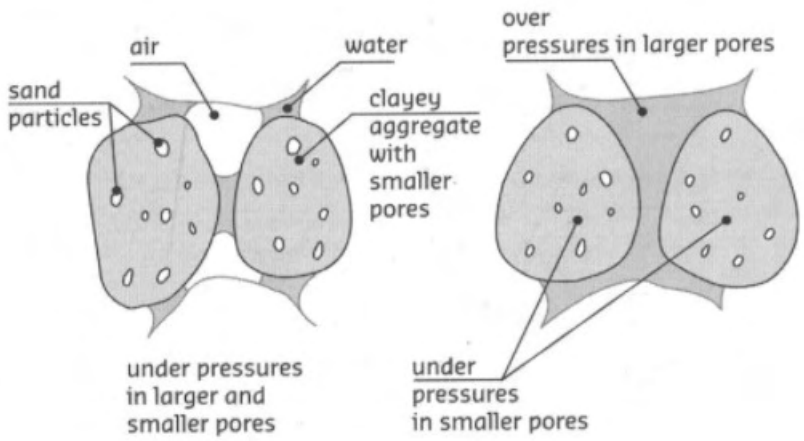

Figure 2.7: Suction pressure in aggregates before and after infiltration. From: Hoffmans (2012)

During overtopping tests (Van der Meer et al., 2015) it was observed that, regardless of the overtopping volume, a water layer was present above the grass cover for 30 seconds after passing of the wave front. When the time between subsequent overtopping events is smaller than 30 seconds, the slope was found to stay wet, causing a fully saturated grass cover as the maximum infiltration capacity was reached. The strength of the grass cover was found to be negatively influenced as a result of these fully saturated conditions (Bijlard, 2015), which was explained to be caused by the decrease in suction pressure.

2.4.4. Fatigue

During a storm, it is possible that waves overtop the crest of a dike. However, after just one overtopping event, the grass cover on the inner dike slope is not very likely to fail. It is often observed that a dike segment fails under repeated wave loading (Steendam et al., 2009, 2012, 2014; Van der Meer et al., 2009a). This suggest the occurrence of material fatigue in grass covers.

Several studies have found that grass covers are susceptible to fatigue damage. Hoffmans (Pijpers, 2013; Steendam et al., 2014) and Bijlard (2015) found that for grass pull tests with a repeated constant displacement, the force required to pull the grass up to that displacement decreased when repeated, which indicates damage accumulation in the grass sod. Van der Meer et al. (2015) performed laboratory fatigue tests and found an increase in residual displacement after repeated loading, a property that characterises fatigue. Wegman used the grass pull test in combination with a stepwise increasing cyclic load regime and found that damage accumulation occurs, as shown by the residual strain in Figure 2.8.

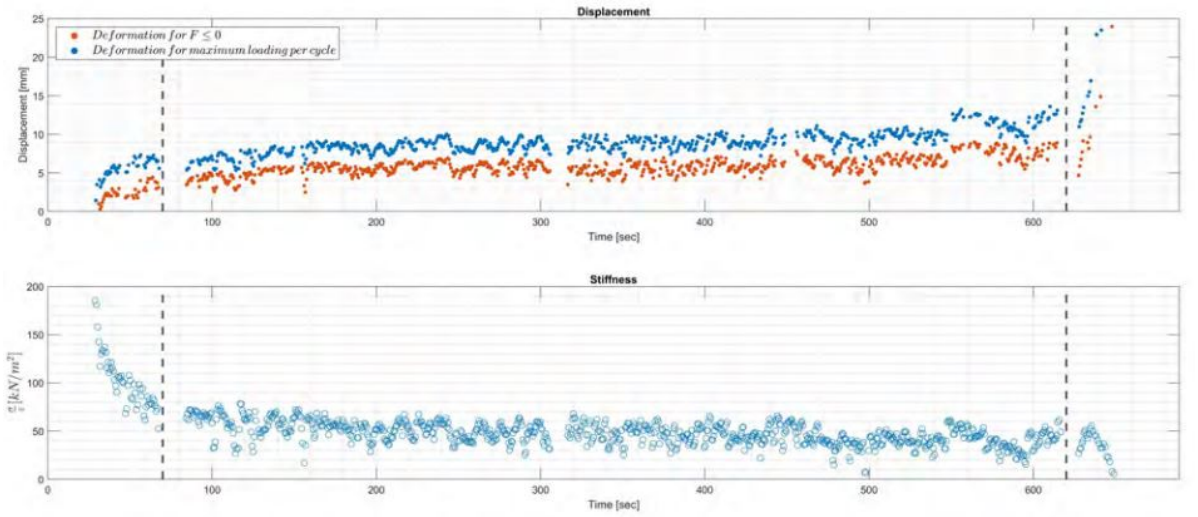

Figure 2.8: Results of the experiment by Wegman (2020). The upper graph shows the displacement as a result of the maximum load (blue line) and the minimum load (orange line). Over time, a residual displacement is found to develop. The lower graph indicates the decrease in elasticity over time. From: Wegman (2020)

Since a grass cover is essentially a composite material made up of multiple components, such as roots, soil, organic matter and more, an analogy may be drawn with other composite materials, such as reinforced concrete or fiber-reinforced plastics. Figure 2.9 shows the strain development for concrete and Figure 2.10 shows the elasticity development for a glass-fiber reinforced plastic laminate. Both materials are subject to fatigue and their behavior during fatigue can generally be described by three different phases, as can be deduced from the figures. These are:

- Phase 1: This phase is characterised by a fast initial residual strain. The elasticity of the sample drops quickly during this phase. The growth of both properties decrease over time however, after which stable growth commences.
- Phase 2: After the fast strain growth from phase 1, the strain development stabilizes, after which the strain grows approximately linearly with time. This also holds for the elasticity of the material, which slowly decreases with time during this phase.
- Phase 3: This phase is characterised by an exponentially increasing strain and as a result, loss of strength. With regards to the elasticity, this property exponentially decreases during this phase. The phase ends with failure of the material.

Both described properties could also be found from the grass pull tests, as can be observed from the results in Figure 2.8 by Wegman (2020).

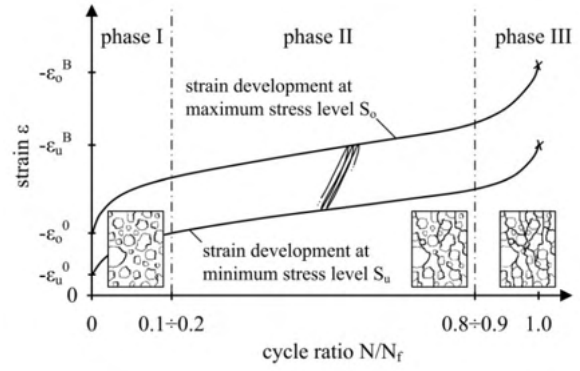

Figure 2.9: Strain behavior as a result of fatigue for concrete. From: Hümme et al. (2016)

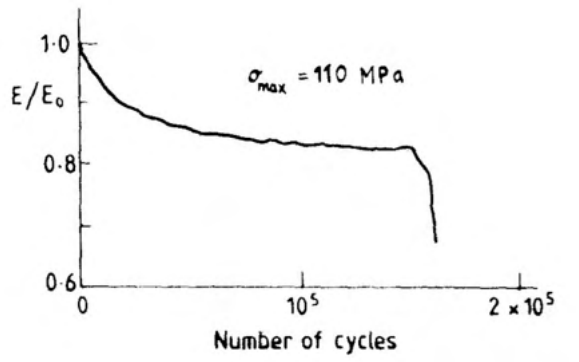

Figure 2.10: Young's modulus reduction as a result of fatigue for a glass-fiber reinforced plastic laminate. From: Ogin et al. (1985)

An important graph in the design of structures that are subject to fatigue is the S-N curve, or Wöhler curve. This is a graphical representation of the data of many performed fatigue tests. To construct an S-N curve, multiple fatigue tests are performed, each at a certain stress amplitude. For each test, the number of cycles till failure is recorded and placed into the diagram. This is done for different load levels. A graph is then fitted to the data to construct the S-N curve. Figure 2.11 shows an example for an S-N curve.

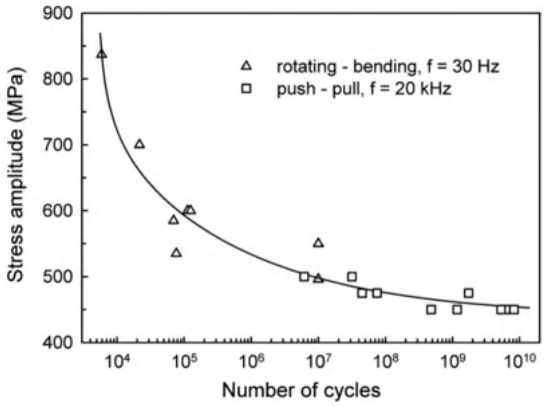

Figure 2.11: S-N curve for a Titanium - Aluminium alloy. From: Janeček et al. (2015)

A downside of the S-N curve is that parameters that influence fatigue behavior, such as loading frequency or temperature are not included. Furthermore, the construction of an S-N curve requires many experiments and is therefore a time consuming and expensive procedure. Hence, alternative methods for the prediction of fatigue life of materials are desired.

Another way of predicting fatigue life is by using the stress-strain diagram of a fatigue test. During fatigue, a material experiences loading and unloading. What is often observed is that the material behaves differently upon loading than upon unloading, as can be observed from Figure 2.12. For loading, the load follows the upper part of the graph until the maximum stress σ_{pp} and maximum strain ϵ_{pp} are reached. For unloading, the strain follows the lower part of the graph back to the origin. This different behavior for loading and unloading is called hysteresis, and it is accompanied by energy loss. The energy loss per unit volume can be calculated from the area inside the hysteresis loop.

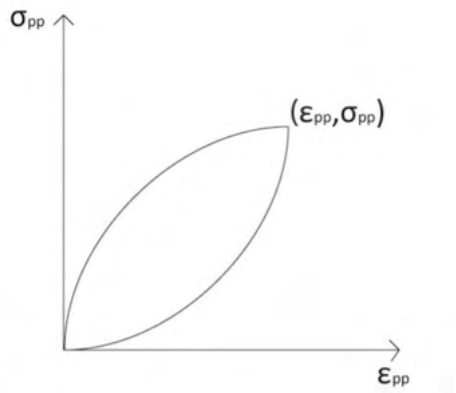

Figure 2.12: Simple description of a stress-strain curve for a load cycle during fatigue. From: Letcher et al. (2012)

Stowell (1966) showed that the total energy dissipation during a fatigue test is approximately equal to the energy dissipation during a monotonic tensile test. The method has been further improved by Scott-Emuakpor et al. (2010) and Letcher et al. (2012, 2011) and resulted in a relatively accurate lower bound prediction for the cycles till failure. However, several assumptions have to be made for the prediction to be valid, and it remains the question whether these are applicable for grass covers.

Another method that may be utilized is predicting fatigue life by means of the strain growth rate. Cornelissen (1984) found the strain growth rate was strongly correlated to fatigue life.

2.5. Erosion models

To mathematically describe the failure of grass covers during wave overtopping, several methods have been developed over the years. Most methods make use of a so called critical velocity, an erosion threshold similar to the criterion of Shields for transport of sediments and stones. When the load, which is the overtopping wave velocity, is larger than this critical velocity, damage is expected to occur.

In the framework of wave overtopping, Dean et al. (2010) proposed several erosion models based on velocity, shear stress and work. Based on these formulations, several other erosion models have been developed, such as the Cumulative Overload Method by Van der Meer et al. (2010) or the Excess Volume Approach by Hughes (2011). As these models are not based on an in-depth physical assessment of grass cover failure, they will not be treated here. More about these models is elaborated in Appendix B. The turf element model by Hoffmans et al. (2009) is treated in this section.

2.5.1. Turf element model

In the Turf element model, Hoffmans et al. (2009) aimed to determine the grass strength based on the equilibrium of vertical forces. The force required to pull a grass sod element out of the cover should be equal or greater than several resisting contributions in the grass sod. For illustrative purposes, the forces acting on the element are displayed in Figure 2.13. The force equilibrium is given by:

$$F_p \geq F_w + 4F_c + F_t \tag{2.20}$$

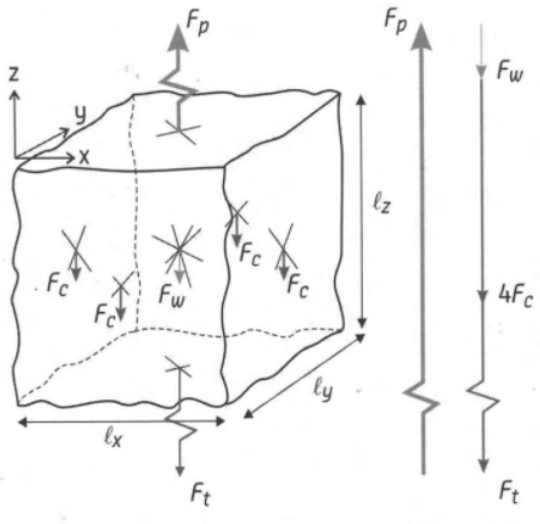

Figure 2.13: Visualisation of the Turf Element Model. From: Hoffmans (2012)

In which F_p is the maximum lift force, F_w is the weight of the sod, F_c are the critical frictional forces on the sides of the sod, which consist of both soil cohesion and root strength, and F_t is the critical mean tensile force on the bottom of the sod. Relating all the parameters together, Hoffmans found for the grass normal stress:

$$\sigma_{soil}(z) = -(1-n)\left[(\rho_s - \rho)gz - 4(C_{clay,c} + \tau_{grass,c}) - (C_{clay,c} + \sigma_{grass,c}(z))\right] \tag{2.21}$$

By applying the Shields criterion, Hoffmans found for the critical shear stress:

$$\tau_c = \Psi_c\left[(\rho_s - \rho)gz + 4(C_{clay,c} + \tau_{grass,c}) + (C_{clay,c} + \sigma_{grass,c}(-\lambda_{ref}))\right] \tag{2.22}$$

In both equations, the n is the porosity, ρ_s and ρ are the soil and water density respectively. $C_{clay,c}$ is the critical rupture strength of clay and $\sigma_{grass,c}$ and $\tau_{grass,c}$ are the critical mean grass normal stress and the critical mean grass shear stress respectively. λ_{ref} is again the reference height, as was given in Equation 2.7.

Hoffmans (2012) assumed that incipient motion starts with the horizontal (shear) forces. For this, the influence of the self-weight of the soil and the soil cohesion were neglected since only the grass was assumed to be able to resist pull forces exerted by the overtopping waves. With this assumption, Equation 2.22 reduces to:

$$\tau_c = \Psi_c \left[4\tau_{grass,c} + \sigma_{grass,c}(-\lambda_{ref}) \right] \tag{2.23}$$

By applying the relation between the shear stress and the turbulence intensity given in Equation 2.2, Hoffmans determined a formulation for the critical velocity, given as:

$$U_c = \alpha_{grass,U} \cdot r_0^{-1} \cdot \sqrt{\frac{\Psi_c(\sigma_{grass,c}(0) - p_w)}{\rho}} \tag{2.24}$$

In this relation, r_0 is the relative turbulence intensity, ψ_c is the critical Shields parameter, $\sigma_{grass,c}$ is the critical mean grass normal stress acting on the surface of the sod, p_w is the suction pressure in the grass sod and ρ is the density of water. $\alpha_{grass,U}$ is a constant correcting for the influence of the critical root grass shear stress and turbulence, which value is about 2.0.

2.6. Numerical models

To gain insight into the physical processes of grass cover failure, as well as for predicting grass cover erosion as a result of wave overtopping, several numerical models have been developed over the years. These models are based on various principles, however, they can be roughly divided into hydrodynamic models and soil stress-based models. To the knowledge of the author, none of the models have proved to be an accurate predictor for grass erosion during wave overtopping, however, they may provide predictive value in combination with other methods or when sufficiently developed.

2.6.1. Hydrodynamic models

Models such as Xbeach or OpenFOAM® focus on the numerical simulation of water motion. Both have been used to get more insight into the stresses and erosion mechanisms of soils with vegetation.

Bendoni et al. (2019) developed an improvement for the Xbeach model to model the effects of vegetation on soil erosion. In this model, the root cohesion as proposed by Wu et al. (1979) is incorporated into the formulation for the critical bed shear stress (Quang and Oumeraci, 2012). The model is able to calculate the change in bed topography based on this relation. Although the model is used to calculate the erosion of salt marshes during wave attack, the concept of including the root reinforcement into the model may be used to simulate grass erosion during overtopping waves.

Additionally, van Bergeijk et al. (2020) developed a model in OpenFOAM® which simulates the wave overtopping flow over a dike inner slope. The model is calibrated by using data of wave overtopping experiments, with good agreement. The model calculates pressures, normal stresses and shear stresses on the dike slope as a result of wave overtopping and was used to identify possible erosion locations during a test case at the Afsluitdijk (Van Bergeijk et al., 2020). The model output consisting of stresses and pressures may be an important step to connect the loads imposed by wave overtopping to the mechanics of grass cover failure.

2.6.2. Soil stress-based models

Soil stress-based models calculated the development of soil stresses as a result of various imposed loads. With these models, insight can be gained into the various failure modes of soil. Van Langevelde (2018) developed a model that calculates the stress development in the soil as a result of a passing overtopping wave. The model uses input parameters such as the Young's modulus, shear modulus and the hydraulic conductivity for the soil stresses to be calculated. Further extension of the model is done by Mersie (2021). Results of the models were found to agree no more than reasonably with overtopping experiments. However, the models serve as a stepping stone for further research.

2.7. Summary

From the literature review, several conclusions can be drawn when considering grass covers:

1. Multiple damage criteria exist for grass covers loaded by overtopping waves. Also multiple attributes that affect grass cover strength are identified, such as root strength, cohesion of the soil and water or suction pressure. However, the available literature does not elaborate on the partial contributions to the grass strength by these attributes. Hence, more insight is desired in how these partial contributions affect grass failure.

2. From the literature review and from field tests it can be concluded that grass covers are susceptible to fatigue damage. However, insight in the fatigue behavior is limited and a quantification of the strength reduction is desired.

3. Numerical models are currently being developed to estimate the erosion of grass covers loaded by overtopping waves. These models are either based on a hydrodynamic approach, in which the load on the bed is investigated, or on a soil stress approach, in which the development of stresses in the soil matrix is investigated. For extension of these models, input parameters are required such as Young's modulus and shear modulus that may be determined by executing grass pull tests.

With these conclusions, experiments are designed to investigate the aforementioned properties of grass covers, which are elaborated in the next chapter.

3

Research method

This chapter elaborates on the tests and equipment that are required to reach the thesis objectives. The grass sod pulling test will be a main instrument for acquiring the data. Hence, it will be described in Section 3.1. Using the grass pull device, it is aimed to get more insight in the various parameters that determine the strength of the grass. This will be done by means of various tests, which will be described in Section 3.2. An overview of the materials required to execute the tests is also listed here. To provide additional information about the root reinforcement of the grass and to relate this to the strength, soil samples have been taken at the locations of the various pull tests. The method is further described in Section 3.3.

3.1. Grass sod pulling test

3.1.1. Device description

The grass pull test device is a device that measures the force and displacement required to pull out a grass sod from a dike cover. The test device consists of a tripod on which an electrical spindle motor is mounted. On the grass sod a pull frame is mounted. From the side of the grass sod, pins are pushed into the sod to attach the grass sod to the pull frame. This pullframe can be connected to the spindle, such that the device is able to pull the grass sod out of the ground. A picture of the pull device is displayed in Figure 3.1a.

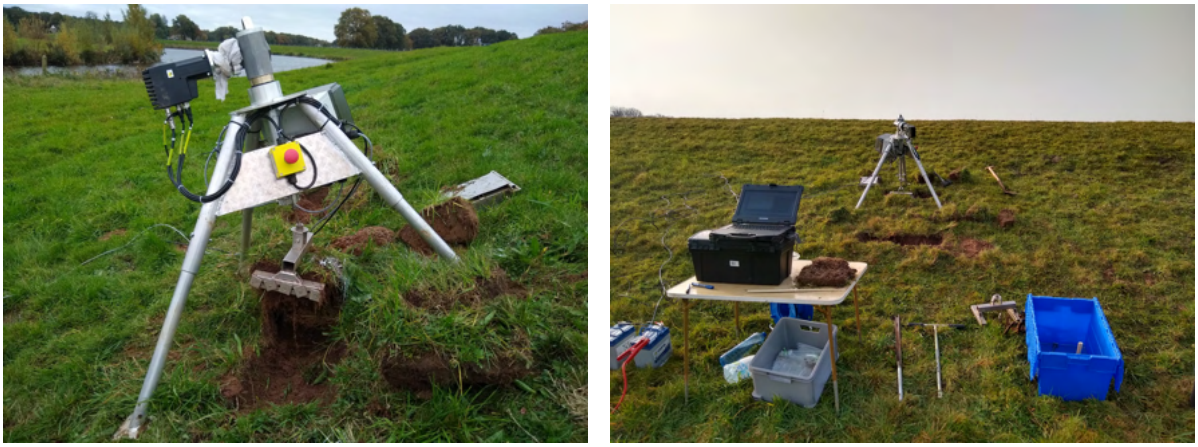

(a) (b)

Figure 3.1: Overview of the grass pull device (a) and of the entire measurement setup during operation (b).

The grass pull device is powered by two 12V VARTA® Blue Dynamic batteries, which are connected to the pull test device by means of power cables. The grass pull device is also connected to a laptop by means of an Ethernet cable. In this way, the grass pull device can be operated by means of a specially developed application. With this application it is possible to define different loading regimes, such as continuous increasing loads or cyclic loads. This can be done by loading a text file with set point values into the application, which may be generated by means of a Python script. The device uses a PID-controller to make sure these desired set point values are transferred correctly to the grass sod. For this, the PID-control parameters have to be given and calibrated by the user. More information about the theory and calibration of the PID-controller can be found in Appendix C. Additionally, the application provides several options to adjust device operation, such as controlling loading speed and whether the test should be force or displacement controlled. The device has a maximum loading speed of 4 cm/s and a sampling frequency of 1000 Hz.

Figure 3.2 shows a description of the execution of a pull test. First a mold is hammered into the soil by using a mallet. The soil around the mold is in turn excavated by using a shovel. After excavation, the mold is removed and the test sample is attached to a pull frame by sliding pins into the pull frame and the sample from the side. After this, the spindle is lowered such that it can be attached to the pull frame. Once the spindle is connected, the pull test can be started.

(a) Mold placement

(b) Excavation around test sample

(c) Installing pull frame

(d) Connecting pull frame to grass pull device

Figure 3.2: Various steps required for the execution of a grass pull test.

3.1.2. Description of test types

Grass pull tests are usually done in two ways; distinction can be made between either the condition 2 test or the condition 4 test. The condition 2 tests will be done with 2 sides cut loose, in order for the pull frame to be installed. The condition 4 tests are done with 4 sides cut loose, hence, the grass sod is only supported from the bottom. An illustration is given in Figure 3.3. The purpose of making a distinction between both tests is to test the contribution of stresses in the side planes. Next to this, both tests can be used to estimate the intact grass sod strength as proposed by the practical method by Bijlard (2015).

(a) Two sides cut loose

(b) Four sides cut loose

Figure 3.3: Overview of the condition 2 and the condition 4 test. The dashed lines indicate the locations where grass cover has been cut. Adapted from: Wegman (2020)

For this research, both test types will be used to investigate the strength contributions of the grass. However some additional test configurations were necessary, upon which will be elaborated in Section 3.2.

To investigate the influence of the saturation of the grass sod, a submerged grass pull tests can be done. For this purpose, the test should be prepared as a normal condition 2 or a condition 4 test by excavating the ground and installing the pull frame. After this preparation, a metal box of 80 x 40 x 20 cm is partly hammered into the soil. After installment, the box is filled with water by means of a pump. The box should be filled well before the execution of the test to make sure the ground and grass are fully saturated. Usually 30 minutes is taken for this to make sure the ground is saturated with water. The submerged test is displayed in Figure 3.4.

(a) Installment of the box

(b) Filling of the box

Figure 3.4: Installment and filling of the box for a submerged test

3.1.3. Metadata

After a grass pull test has been executed, metadata has been recorded into an Excel-file to provide data regarding the test conditions. This metadata is important since it provides information to correct the pull test data and to rewrite the variables in terms of stresses. Comments on the performed tests are also given in these metadata files, in case strange results for the grass pull tests are obtained. The metadata can thus be used to check what may have caused deviation from regular test results. The metadata that is recorded in these files consist of:

- Test number
- Time and date of test execution
- Test condition (condition 2 or 4)
- Dike orientation
- Weather conditions
- Sod weight
- Sod thickness
- Sod width
- Root length
- Pictures of the sample

The measuring of sod thickness, sod width, root length and the making of pictures are done after the test has been executed. Determination of the sod width is done by using a yardstick. For the determination of the thickness and the root length of the sod, a special procedure is adopted, since the sod thickness as well as the root length vary largely over the sod. First, three main areas are identified on the bottom of the sod. The sod thickness in each area should approximately be the same and all three areas should together cover 100% of the sod bottom surface. With the yardstick, the thickness of these three areas is measured. After measuring the thickness, the mean root length for each area is determined by measuring some of the roots with the yardstick and thereby estimating the mean root length for that particular area. Figure 3.5 visualizes how the areas are determined.

(a) Variation in sod thickness

(b) Method to determine the sod thickness

Figure 3.5: Variation of the sod thickness and root length. The method to determine the sod thickness is described in (b).

3.1.4. Subsidence of the pull device

During a grass pull test, the tripod was found to pull itself into the soil as a result of the pulling force. This subsidence was generally in the order of a couple of millimeters, however, since it could affect the results of the data analysis, the amount of subsidence was measured. To do so, ground pegs were put into the ground on the locations where the tripod feet were placed on the ground. After a pull test, the distances between the top of the ground pegs and the top of the tripod feet were measured. The correction was then done by means of a script containing a trigonometric algorithm, using the measured subsidence per leg as input.

3.2. Description of various tests

To understand how erosion to a grass cover can occur, it is important to know what parameters contribute to the grass cover strength. Therefore, it is aimed to investigate the influence of these parameters by performing various grass pull tests, in order to find various contributions to the strength. From the literature review it was found that more insight is desired in the behavior and quantification of various strength contributions. Furthermore, several material properties may be deduced from the grass pull test, which in turn may be used as input for numerical models. Summarizing, the influence on the strength by the following attributes is of interest:

- Soil type (sand or clay)
- Saturation with water
- Cohesion of the soil
- Fatigue
- Root reinforcement
- Material properties

Since the grass cover strength is depending on stress components from all directions in the three dimensional space, it was aimed to isolate every component and investigate its relative contribution to the grass cover strength. The Turf Element Model as proposed by Hoffmans (2012) served as a main inspiration for this approach. Based on the mentioned interests and concepts, various experiments were designed to get insight into these properties of grass covers. These are:

- Normal pull tests
- Shear tests
- Stepwise increased constant load tests
- Fatigue tests
- Root counts

Table 3.1 gives an overview of the tests and the attributes that could be investigated per test. From Table 3.1 it could be observed that for all tests types the influence of saturation could be investigated, as well as the difference between a non-cohesive sandy subsoil or a cohesive clayey subsoil. For the fatigue tests however, many tests were desired to be executed. Due to time constraints, it was chosen to perform all fatigue tests under submerged conditions, since this mimics the actual failure mechanism of waves overtopping a grass cover.

Attribute of interest	**Normal pull test**	**Stepwise constant test**	**Shear test**	**Fatigue test**	**Root counts**
Fatigue	-	X	-	X	-
Influence of saturation	X	X	X	X	-
Difference sand vs clay	X	X	X	X	X
E-modulus	X	-	-	-	-
G-modulus	-	-	X	-	-
Influence of roots on strength	X	X	X	X	X

Table 3.1: Attributes of interest and the types of experiments that may be used to investigate them.

A more in depth description per test type will be given in the subsequent sections.

3.2.1. Normal pull tests

In the Turf Element Model of Hoffmans (2012), normal stresses at the underside of the sod provide a contribution to the total strength of the grass cover. To investigate the strength contribution of the normal stress at the bottom of the grass sod, normal pull tests are performed. The normal pull test is conducted as a condition 4 test and is displacement controlled, in which the displacement of the spindle increases linearly with a speed of 1 cm/s. While the grass sod is being pulled, the device measures the force and displacement. With the forces, displacements and dimensions of the grass sod known, a stress-strain curve can be obtained, from which it is possible to derive the modulus of elasticity, as given by:

$$E = \frac{\sigma}{\epsilon} \tag{3.1}$$

In which σ is the stress and ϵ is the strain. The stress is defined as:

$$\sigma = \frac{F}{A} \tag{3.2}$$

In this equation, F is the normal force and A is the surface on which this normal force acts. The strain is defined as:

$$\epsilon = \frac{\Delta l}{l} \tag{3.3}$$

In which Δl is the extension of the material in the normal direction and l is thickness of the test sample, as determined by the method described in Section 3.1.3.

Material behavior is often described by Hooke's law, which states that its deformation is directly proportional to the force on the material, with the modulus of elasticity being the proportionality constant. Therefore, Hooke's law is only valid when the stress-strain relation is linear. For the normal pull tests, this was found not to be the case. Hence, other formulations for the modulus of elasticity are adopted, such as $E_{50\%}$ and E_{peak}, which are essentially secant moduli. These are defined as follows:

$$E_{50\%} = \frac{\sigma}{\epsilon_{50}} \tag{3.4}$$

$$E_{peak} = \frac{\sigma}{\epsilon_{peak}} \tag{3.5}$$

In these relations, ϵ_{50} is the strain at 50% of the peak strength and ϵ_{peak} is the strain at peak strength. Validation of the obtained values is done by comparing the calculated values to values in literature.

3.2.2. Shear tests

In the Turf Element Model of Hoffmans (2012), shear stresses provide a large contribution to the strength of the grass cover. To investigate the shear strength of a grass cover, shear tests have been performed. Similarly to the normal pull tests, the shear tests are also performed as a displacement controlled test, in which the speed is set to 1 cm/s. For this type of test, the grass is cut over a longer stretch. A plane located 8 cm underneath the grass cover is cut, such that the grass is not supported anymore in the vertical direction. By doing so, the idea is that the grass is only loaded by shear forces on the two shear planes on the top and bottom of the picture. To make sure both planes are entirely loaded with a shear force, the sides are fixated to the ground by means of wooden beams and cramps. Extra metadata was recorded to locate the failure planes. With the obtained forces, displacements, dimensions and failure plane locations, a stress-strain curve could be obtained. From the obtained parameters it is possible to determine the shear modulus, which is defined as:

$$G = \frac{\tau}{\gamma} \tag{3.6}$$

In Equation (3.6), τ is the shear stress and γ is the shear strain. The shear stress is defined as:

$$\tau = \frac{F}{A} \tag{3.7}$$

In this equation, F is the shear force and A is the surface on which the shear force acts. The shear strain is defined as:

$$\gamma = \frac{\Delta x}{l} \tag{3.8}$$

In which Δx is the extension perpendicular to the normal and l is the horizontal length of the block that deforms. Figure 3.6 shows an example of the shear test execution.

(a) Excavation for the shear test

(b) Submerged configuration for the shear test

Figure 3.6: Shear test execution

3.2.3. Stepwise increasing constant load tests

To investigate the time-dependent effect of the grass strength, stepwise increasing constant load tests are performed. In this test, the load is increased in a stepwise manner, after which it is held constant for a time interval of 10 minutes. During the test, the displacement is measured by the grass pull device. By doing the test in this manner it is aimed to provide insight in how the strain will develop over time and whether it differs between the two soil types. The load regime is depicted in Figure 3.7.

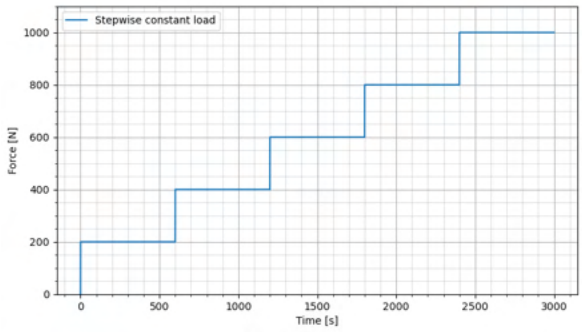

Figure 3.7: Load regime for the stepwise increased constant load tests

Since the strain development will be the main interest during this test rather than the strength, the test is performed as a condition 2 test. The tests are performed for both dry and submerged conditions.

3.2.4. Fatigue tests

To determine to what extent grass is influenced by fatigue, fatigue tests have been done. Wegman (2020) already performed fatigue tests and showed that a grass cover was influenced by fatigue. However, the grass pull device was manually operated and the loads deviated from the intended load regime. Therefore, the fatigue tests are repeated to more accurately investigate the effect of repeated loading on the grass cover. However, the investigation will be executed in two steps.

In the first step, it is aimed to investigate at what load levels grass covers would fail under fatigue. For this the stepwise increasing cyclic loading scheme was adopted, as proposed by Wegman (2020). The loading regime is shown in Figure 3.8a.

The second step consists of doing many measurements at a constant cyclic load. The measurements are performed until failure or until it was found that testing would take too long. The ultimate goal of this approach is to create a partial or full S-N curve for a grass cover. The constant cyclic loading regime is displayed in Figure 3.8b.

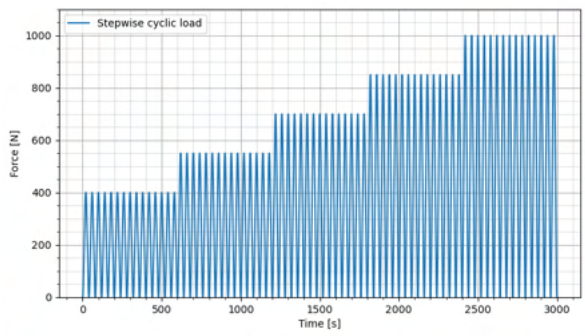

(a) Stepwise cyclic loading scheme as used during the fatigue tests.

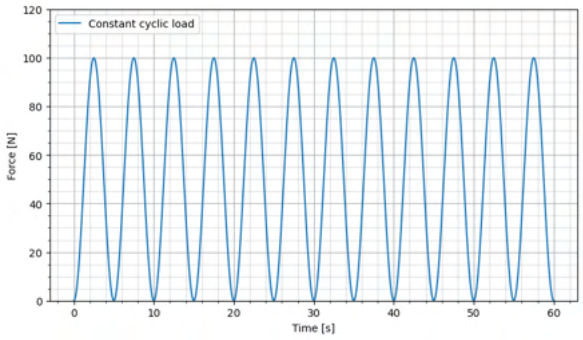

(b) Cyclic loading scheme as used during the fatigue tests.

The main objective for the fatigue tests is to investigate the material behavior during fatigue and to investigate the decrease in tensile strength. The decrease in strength may be used in some erosion models, such as the relation by Hoffmans (2012) for determining the critical velocity.

For the period of the cyclic load during the fatigue tests, a period of 5 seconds was used. To justify this frequency, several reasons are mentioned below:

- The frequency of loading is depending on the limits of the grass pull device. As was mentioned in Section 3.1, The grass pull device has a maximum loading speed of 4 cm/s. The fatigue test is executed as a force-controlled test, which is operated by the PID-controller. Wrong calibration for the PID-controller could lead to possible overshoots. With a slow varying load, this could still happen, however is less likely.
- Overtopping waves generally have periods that lie in the 5 second range, and hence it seems more appropriate to use a loading regime that is reminiscent of the actual loading regime as found during wave overtopping.
- Fatigue is more severe under a slow varying load, hence lower frequencies will lead to earlier damage. This is beneficial for testing since failure will occur earlier on, leading to less time required for the experiment.

3.3. Root counts

To investigate the influence of the grass roots on the strength of the cover, soil samples have been taken at the locations of the various pull tests. This is done by means of a gouge with a diameter of approximately 3 cm, which is forced into the ground. From the soil samples, the amount of roots could be counted, after which the number of root over the depth could be obtained. Based on the amount of roots, the grass cover quality can be determined, as well as the influence of the roots on the grass strength. The root counts have been done according to the VTV2006 report (Ministerie van Verkeer en Waterstaat, 2007), as described in Section 2.3.3. A picutre of a soil sample is displayed in Figure 3.9.

Figure 3.9: Soil sample in a gouge, to be used for root counts

4

Results

This chapter treats the results of the various experiments and analyses performed to reach the thesis objectives. In total, 180 tests have been performed during these measurement campaigns, spread over the Vechtdijk, the Waddenzeedijk and the Prosperdijk. Table 4.1 presents an overview of the number of tests that are performed, arranged by test type and test location. Measurements have been performed from the 22nd of February until the 29th of March of 2021. In Appendix D, E and F, the individual test results are displayed for the measurement series performed at the Vechtdijk, the Waddenzeedijk and the Prosperdijk respectively.

Type of test	**Vechtdijk**		**Waddenzeedijk**		**Prosperdijk**
	Dry	Submerged	Dry	Submerged	Submerged
Normal pull test	14	11	10	10	-
Shear test	11	12	10	10	-
Stepwise increased constant test	11	10	10	10	3
Stepwise increased fatigue test	-	3	-	-	3
Constant fatigue test	-	19	-	10	-
Stepwise shear fatigue test	-	3	-	-	-
Shear fatigue test	-	4	-	6	-

Table 4.1: Overview of the performed tests

Section 4.1 treats the results of the normal pull tests and the shear tests and discusses the determination of the Young's and shear modulus. Section 4.2 treats the influence of the pore saturation, root reinforcement and the subsoil type on the failure mode of the grass cover. They are treated in the same section as it was found that these parameters affected each other. Fatigue characteristics of the grass cover are treated in Section 4.3.1 while Section 4.4 treats prediction of fatigue. Since a relatively equal amount of tests have been performed on both a sand dike as well as a clay dike, as can be observed from Table 4.1, each section will be treating the differences observed between sandy and clayey grass covers as well.

For some tests, measurement errors made the data unsuitable for analysis, as results from these tests would not be accurate. This is the reason why in some of the graphs some tests from a measurement series are missing. Section 5.4 of chapter 5 treats the sources of these measurement errors.

4.1. Strength analysis and material properties

In this section, the results for the normal pull tests and the shear tests are discussed. Both tests are inspired by the Turf Element Model by Hoffmans (2012) to investigate the strength contributions on the various sides of the grass sod. Furthermore, as found from the literature, the modulus of elasticity and the shear modulus are material properties that may be used as input for numerical erosion models. This section also elaborates on the determination of these parameters.

4.1.1. Normal pull tests

Figure 4.1 shows the stress-strain relation for all test series of the normal grass pull tests. What can be observed from the figure is that for sand, the grass cover seems to retain some strength after the maximum strength level has been reached, as the strength peak is relatively drawn out. For clay however, it can be observed that after reaching peak strength, the stress value in the curve drops quickly, implying that little strength is retained after the peak strength. This suggests that the failure mode for clay is relatively brittle, while the failure mode for sand seems to be more tough. Also, the strain required for reaching peak strength is generally less for clay than it is for sand. Hence, the stress-strain relation shows a steeper rise for clay than for sand, which results in a larger modulus of elasticity.

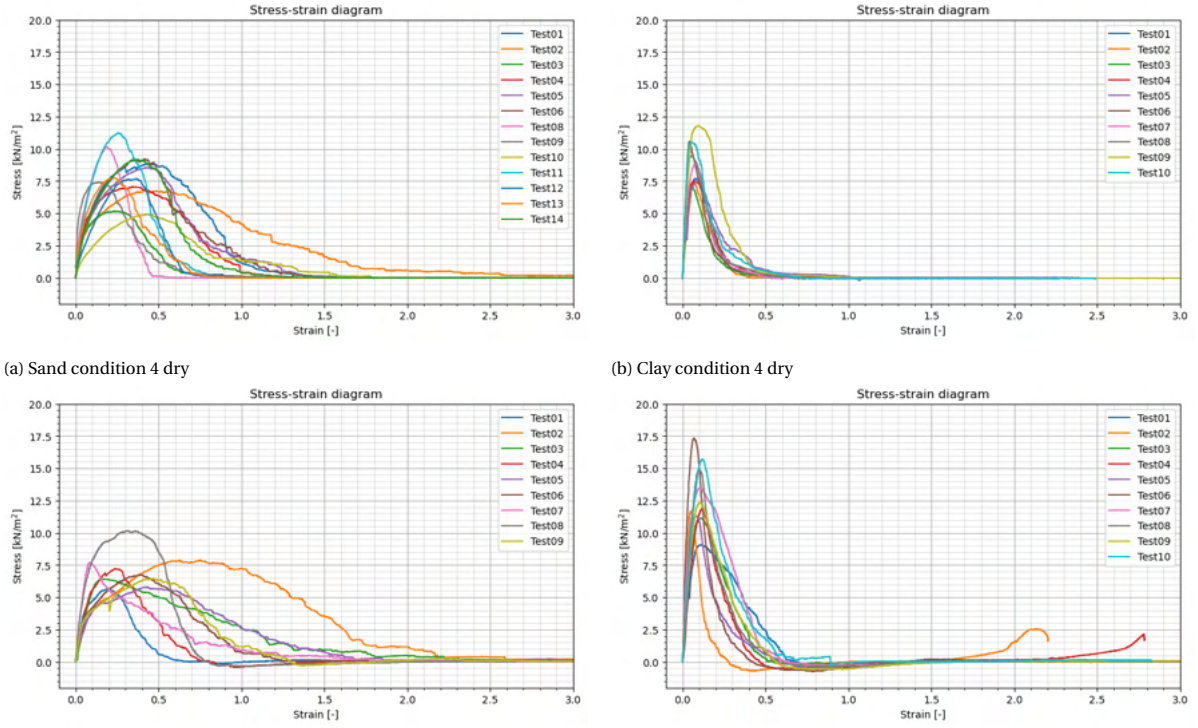

(a) Sand condition 4 dry

(b) Clay condition 4 dry

(c) Sand condition 4 submerged

(d) Clay condition 4 submerged

Figure 4.1: Stress-strain diagrams for the four normal pull test measurement series.

Figure 4.2 shows the variation in the tensile strength for both the normal pull tests and the stepwise increasing constant load tests. Note that the stepwise increasing constant load tests are executed as condition 2 tests instead of condition 4 tests. For non-submerged conditions, it could be observed that for both test types, there is little difference between the magnitudes of the tensile strength, although it could be observed that the spread for sand is a little larger than for clay. For submerged conditions however, some differences can be observed. For a sandy subsoil, the dataset shows a lower strength for submerged conditions than for non-submerged conditions. For a clayey subsoil, this is not the case; A higher strength is observed for the normal pull tests, while for the stepwise increasing constant load tests a lower strength is observed in comparison with non-submerged conditions. This is not expected, since stepwise increasing constant load tests are executed with two sides intact, while for the normal pull test all sides are cut. For these reasons, stepwise increasing constant load tests are expected to provide larger strength.

Apparently, the time scale in which the load is imposed on the grass cover plays a role. The normal pull tests have been executed as quick tests, while the stepwise increasing constant load tests are performed as long duration tests. The quick loading mechanism seems to strengthen the grass sod during submerged conditions, while the long lasting load mechanism causes weakening.

A possible explanation for the phenomenon may be the fact that the pores in the test sample expand as a result of the instantaneous pull force caused by the grass pull device. This phenomenon is known as dilatancy. As a result of this rapid pore expansion, the water that occupies theses pores may experience a drop in pressure, which strengthens the sample. This causes the surrounding water to flow towards the low pressure area, eventually filling the enlarged pores and diminishing the negative pressure. The long time required for failure of the stepwise increasing constant load tests may allow the low pressures developed by dilatancy to diminish, effectively decreasing the grass strength. This may explain the differences observed in Figure 4.2. The hypothesis is reflected upon in Chapter 5. The phenomenon may also occur for sand, however this is not visible from the graph.

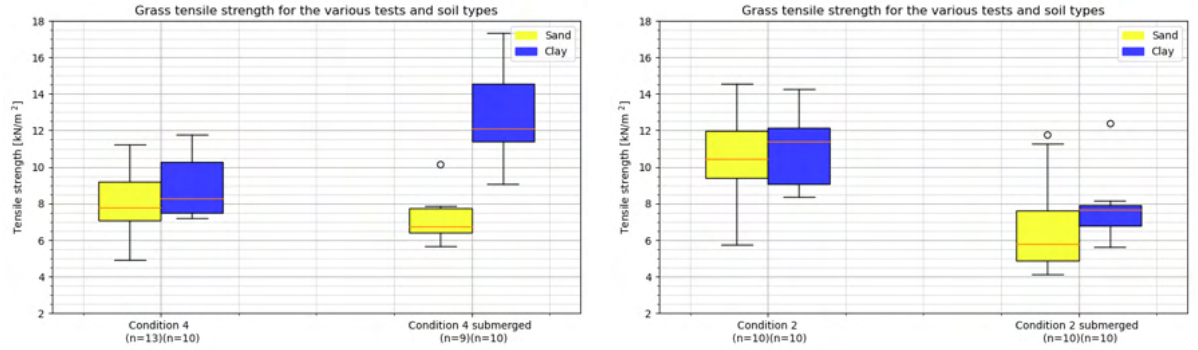

(a) (b)

Figure 4.2: Boxplots displaying the variation of tensile strength for the normal pull test (a) and for the stepwise increasing constant load test (b).

4.1.2. Modulus of elasticity

The modulus of elasticity was determined from the stress-strain relation for each individual normal pull test. Figure 4.3 shows an example of such a stress-strain relation, with both $E_{50\%}$ and E_{peak} determined by using Equation 3.4 and 3.5 from Section 3.2.1.

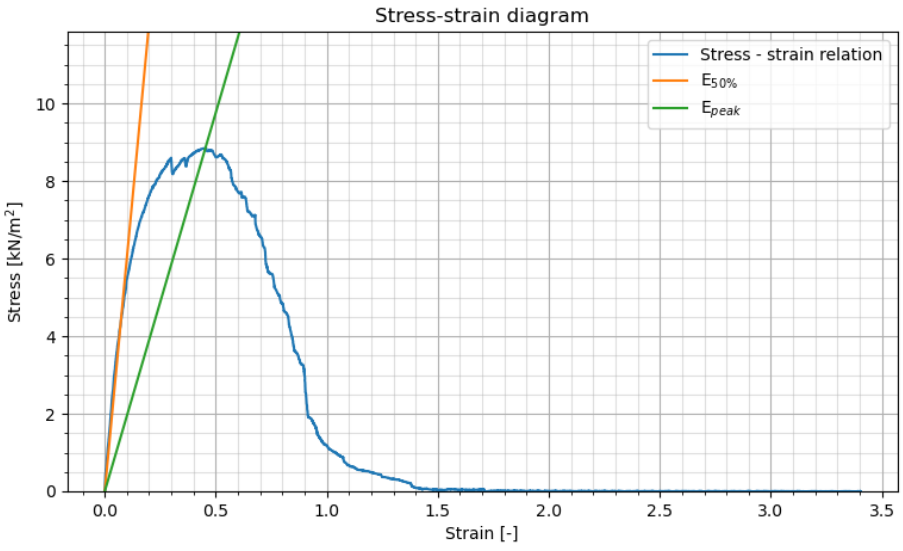

Figure 4.3: $E_{50\%}$ and E_{peak} determination using the stress-strain relation of a normal pull test.

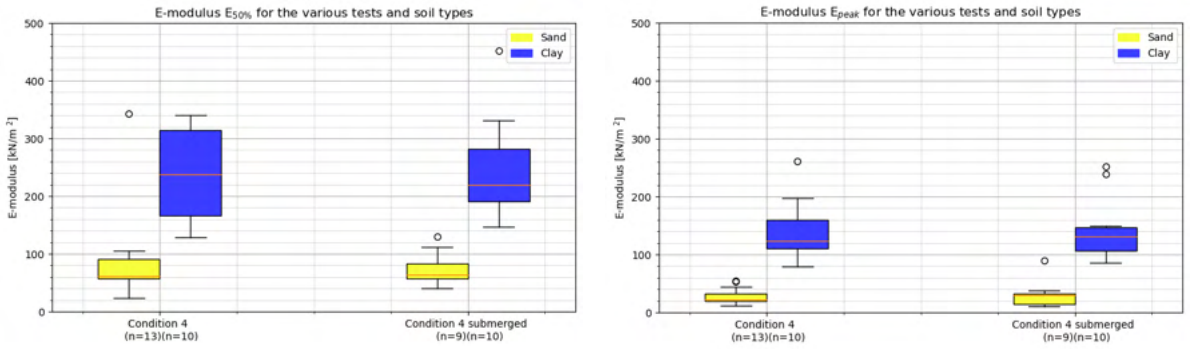

(a) (b)

Figure 4.4: Boxplots displaying $E_{50\%}$ (a) and E_{peak} (b), as determined with the normal pull test.

All calculated elastic moduli determined by using the normal pull tests are displayed in the boxplot of Figure 4.4. For both elastic moduli, it can be observed that a clayey subsoil seems to provide more stiffness to the grass cover than a sandy subsoil, implying that more force is required to deform clayey grass covers. Additionally, the elastic moduli for clay show a larger spread when compared to the elastic moduli for sand. The differences in stiffness could also be observed from Figure 4.1.

4.1.3. Shear tests

During the shear test, the test sample is connected to the surrounding grass on two sides. While pulling, two failure planes develop during the test, which can be identified as two distinguishable strength peaks in the shear stress-shear strain diagram. It should be noted that the second shear peak has no value, as after development of the first failure plane, the pull frame tumbles over. This causes the load mechanism to deviate from pure shear conditions. Hence, the second shear peak is not representative for shear analyses. Therefore, the strength analyses in this section are based on the first strength peak only.

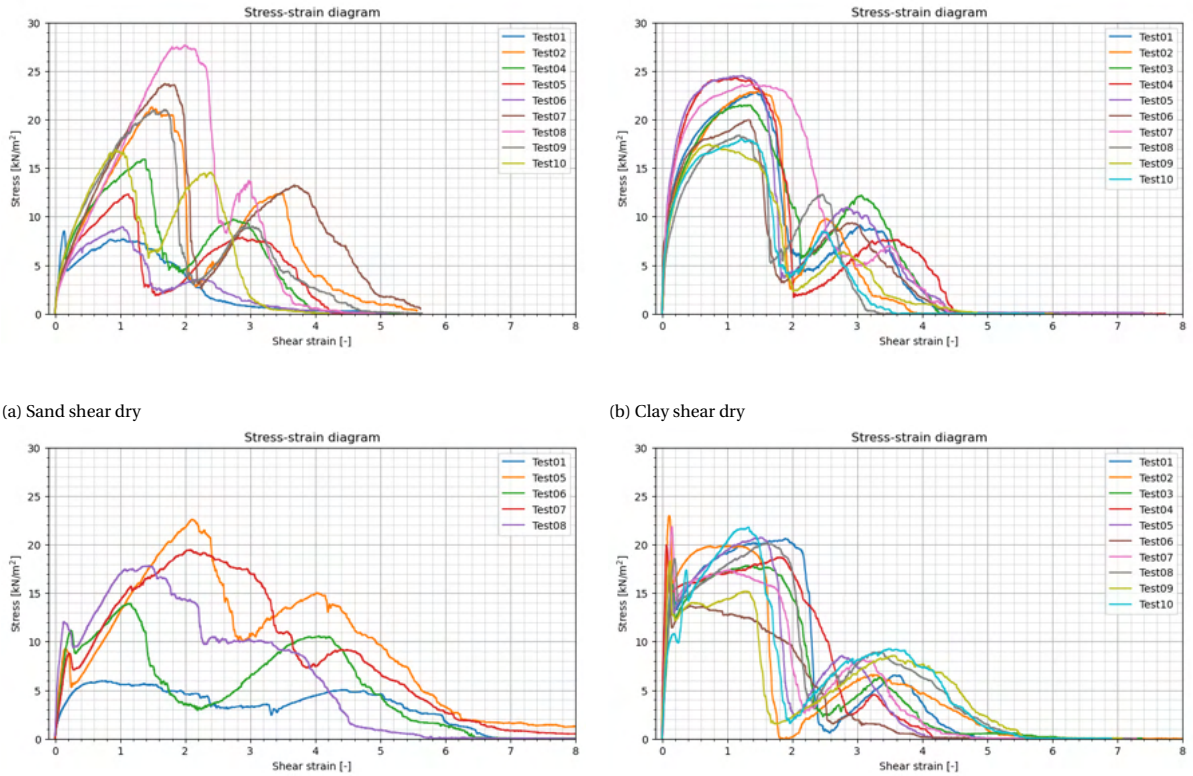

(a) Sand shear dry

(b) Clay shear dry

(c) Sand shear submerged

(d) Clay shear submerged

Figure 4.5: Stress-strain diagrams for the four normal pull test measurement series.

The shear stress-shear strain diagrams for all test series have been plotted in Figure 4.5. From the figure, several things can be observed. First of all, a remarkable finding can be made when looking at the submerged shear tests in Figure 4.5; A third strength peak can be found shortly after the start of a submerged shear test. This is observed for almost all submerged shear tests. Since the third strength peak is absent for the dry test, it is likely that this has to do with the submerged conditions. The dilatancy hypothesis as proposed in Section 4.1.1 may explain the occurrence of these strength peaks, as the shear stresses on the failure planes may cause pore expansion to occur. The pore expansion may in turn cause the development of negative pore pressures, leading to strengthening of the grass sod. As the grass was not found to be failing during these strength peaks, the observed strength peaks have been excluded from the strength analyses. However, especially for clay, the strengthening during these peaks is observed to be considerable. For sand, the peaks are also visible, however they are generally lower than those for clay. The larger permeability of sand may serve as an explanation for these lower peaks, as suction pressures dissipate more easily in high permeability soils.

When looking at the dry shear tests, the sandy grass cover seems to approach peak stress more linearly, while the clayey grass cover seems to approach peak stress more parabolically. A possible explanation for the different behaviors may be caused by the differences in soil properties. For clay, the shear strength is most likely determined by both cohesion and root reinforcement. This causes a steep initial slope, similarly to the observations for clay in Figure 4.1. After this steep initial growth, the grass sod deforms while the stress level does not increase much anymore, such that a decrease in stiffness is observed. For sand, cohesion is absent, however some resistance against shear is still present due to internal friction between the sand grains. Still, it is likely that the roots are mostly responsible for the shear strength in sandy grass covers. Due to the absence of cohesion, the initial slope is therefore less step than that for clay. Failure is however instantaneous for both soil types, as is shown by the quick drop of stress after peak strength. This was also observed in the field, with the test sample rupturing rapidly.

Figure 4.6 shows the shear strength and the shear strain at maximum strength. With regards to the shear strength, clay is generally found to be stronger than sand. Additionally, the submerged conditions cause a shear strength reduction for both sand and clay. The observation of a strength reduction was also found for the normal pull tests and the stepwise increased constant load tests, although clay under submerged conditions was found to be stronger. Furthermore, both materials seem to be failing at roughly the same values for the shear strain, as is shown by the median values from Figure 4.6. However, the spread in results is relatively large, with dry clay being the only material having little variation in the results.

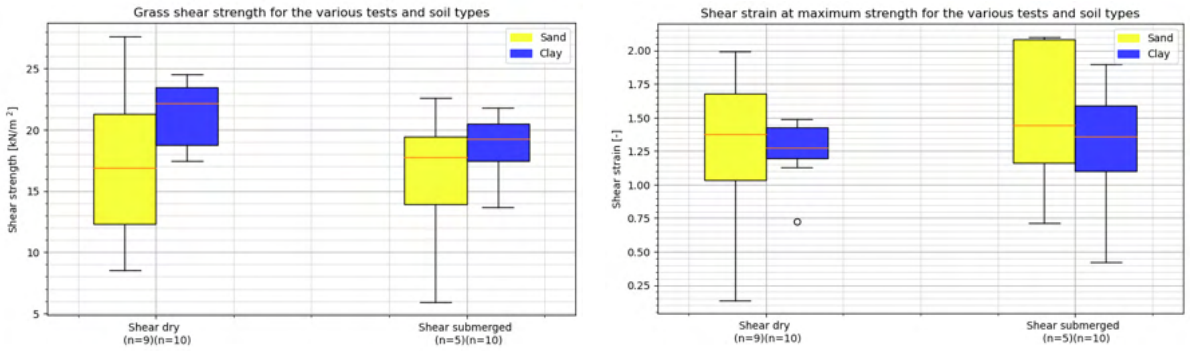

(a) (b)

Figure 4.6: Boxplot displaying the variation of the shear strength (a) and the shear strain (b) for the shear test.

4.1.4. Shear modulus

The shear modulus was determined from the shear stress-shear strain relation for each individual shear test. Figure 4.7 shows an example of such a shear stress-shear strain relation, with G determined by using Equation (3.6) from Section 3.2.2.

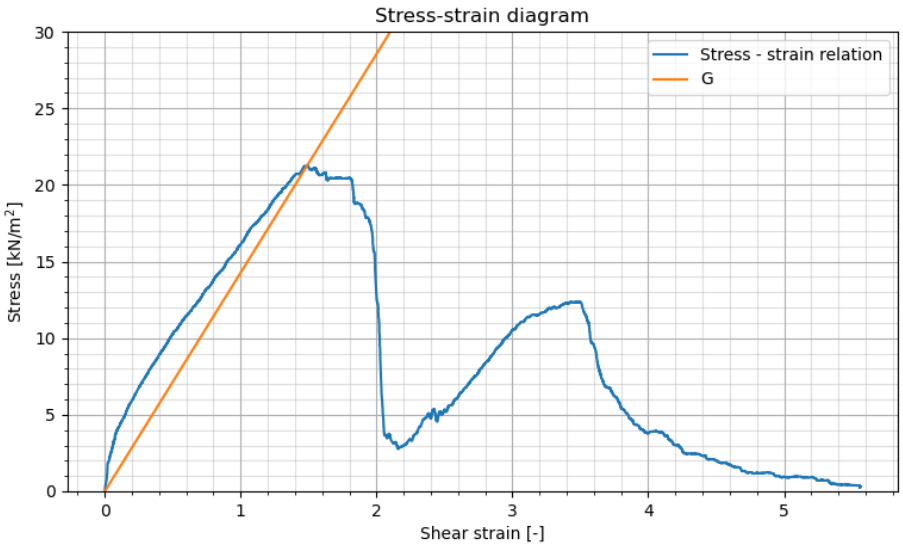

Figure 4.7: G determination using the shear stress-shear strain relation of a shear test.

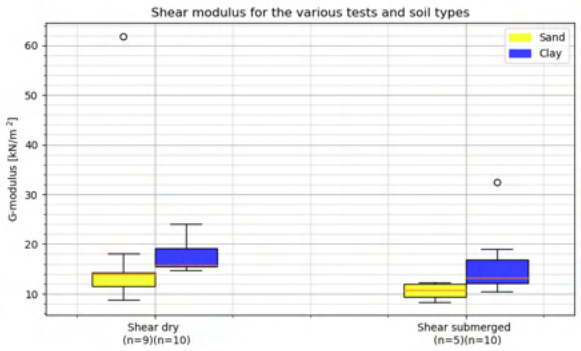

Figure 4.8: Boxplot displaying the values for the shear modulus G, as determined with the shear test.

The calculated shear moduli determined with the shear tests are displayed in the boxplot of Figure 4.8. From the boxplot, it can be observed that shear moduli are slightly larger for clayey grass covers than for sandy grass covers, implying that more force is required to deform clayey grass covers. For submerged conditions, values are slightly lower than for dry conditions, as can be observed for both soil types. To conclude this section, an overview of the calculated Young's and shear moduli is provided in Table 4.2.

	Mean [kN/m^2]	St. dev. [kN/m^2]	95% conf. int. upper bnd. [kN/m^2]	95% conf. int. lower bnd. [kN/m^2]
Sand dry				
$E_{50\%}$	89.44	76.53	131.05	47.84
E_{Peak}	28.01	13.56	35.39	20.64
G	18.42	15.55	28.58	8.26
Sand submerged				
$E_{50\%}$	73.67	27.94	91.92	55.41
E_{Peak}	30.73	22.95	45.72	15.74
G	10.56	1.53	11.9	9.22
Clay dry				
$E_{50\%}$	237.63	78.42	286.23	189.02
E_{Peak}	140.75	51.67	172.78	108.73
G	17.43	3.08	19.34	15.52
Clay submerged				
$E_{50\%}$	245.12	87.29	299.22	191.02
E_{Peak}	144.62	53.88	178.02	111.23
G	15.7	6.2	19.54	11.85

Table 4.2: Overview of the calculated Young's and shear moduli for the various test conditions.

4.2. Influence of pore saturation, roots and subsoil type on failure modes

From the strength analyses performed in the previous section, it could be observed that the grass is generally weaker under submerged conditions. However, some anomalies during submerged conditions were found, such as the results for the normal pull tests for clay and the submerged shear tests. The stiffness of the material was found to decrease slightly during submerged conditions, as could be observed from the results for the Young's and shear moduli.

To check the influence of the root reinforcement on the grass cover strength, soil samples have been taken at the location of the grass pull tests according to the method described in the VTV2006 report. The roots in these soil samples have been counted for multiple layers, after which root profiles could be obtained. Note that root profiles are only generated for a limited number of normal pull tests, as the counting procedure was found to be very labor intensive. As a result, 55 root profiles are generated for sand while 15 root are generated for clay. In Figure 4.9, the mean and the 95% confidence interval of these obtained root profiles are plotted for the sandy Vechtdijk and the clayey Waddenzeedijk respectively. With the plot, information can be gained about the quality of the grass cover.

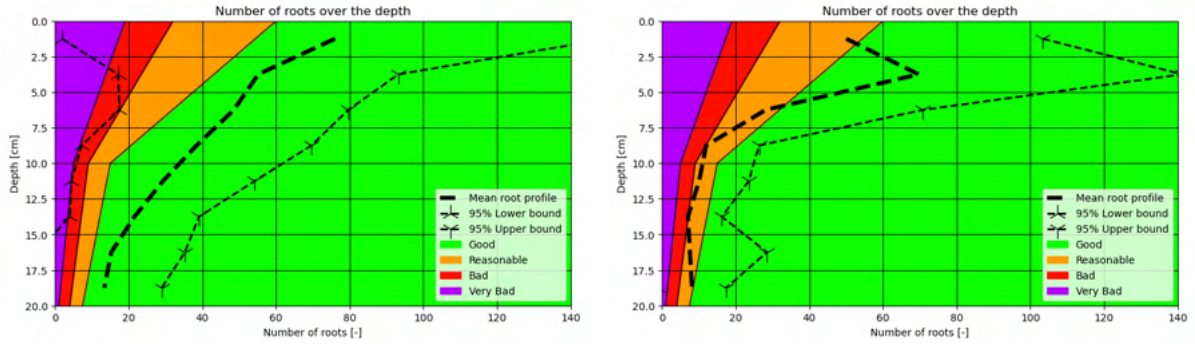

(a) (b)

Figure 4.9: Mean and confidence intervals for root profiles for the sandy Vechtdijk (a) and for the clayey Waddenzeedijk (b).

From Figure 4.9f, it can be seen that the 95% confidence intervals indicates that the spread in the root counts is considerable. For clay, the lower bound of the confidence interval is not plotted as the spread causes the lower bound to become negative. Furthermore, the figure highlights some differences in the root profile between sand and clay. For sand, the number of roots seem to decrease with depth relatively evenly. However, for clay, a large decrease in the number of roots in the lower four to five layers is observed. A possible explanation for this is that the roots in clay may have more difficulty with penetrating the soil as they grow. As a result, mainly the top layers are thoroughly rooted. From the plot, the large spread as highlighted by the confidence interval makes it difficult to asses the quality of the grass cover, although the mean root profiles indicate that the grass cover quality is better for the Vechtdijk.

In Figure 4.10, the root profiles are plotted versus their corresponding tensile strength, as determined with the normal pull tests. For a certain strength level found with the grass pull test, the corresponding root profile is visible in the diagram as eight colored dots that are spaced horizontally, with each dot representing the number of roots in that particular layer. From the theory, a positive correlation is expected, indicating that a higher number of roots in the grass sod should lead to a higher tensile strength. As can be observed in the graphs, the spread is considerable, which may be explained by the large spread as observed in Figure 4.9. Furthermore, layers samples which contain a larger number of roots do not necessarily show a larger corresponding strength. Based on these results, it could not be concluded whether an increase in the number of grass roots causes higher grass cover strength. A possible explanation for not finding a correlation may be caused by the method by which the root counts are performed. This is highlighted in more detail in Section 5.4.4. Other explanations may be that grass strength is more determined by the tensile strength of the roots rather than by the number of roots in the sample. Since roots have multiple diameters, a grass sod with few but large roots may be stronger than a grass sod with many but small roots. Furthermore, the grass cover strength is not solely dependant on root reinforcement, but on other parameters as well, such as the degree of pore saturation and the subsoil type. It is possible that there is an optimum of root reinforcement in relation to these parameters.

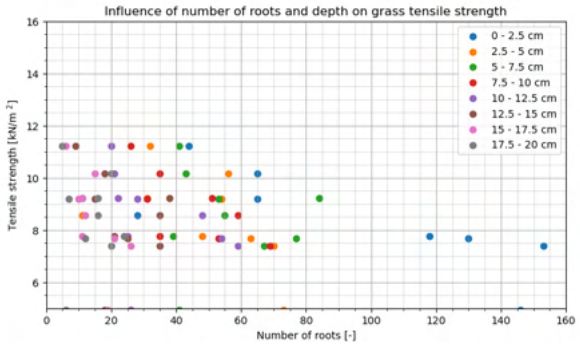

(a) Sand condition 4 dry

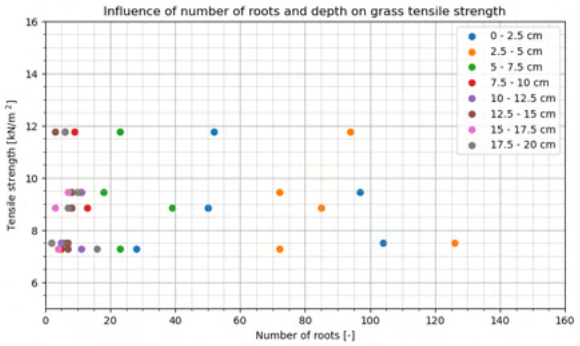

(b) Clay condition 4 dry

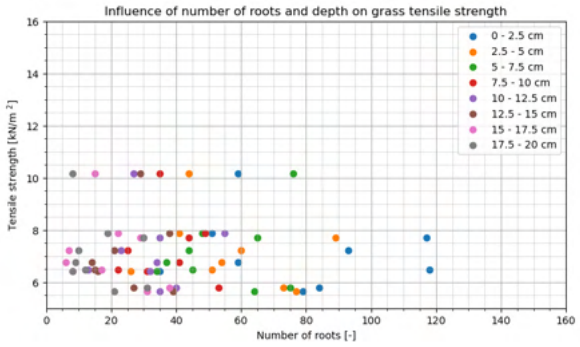

(c) Sand condition 4 submerged

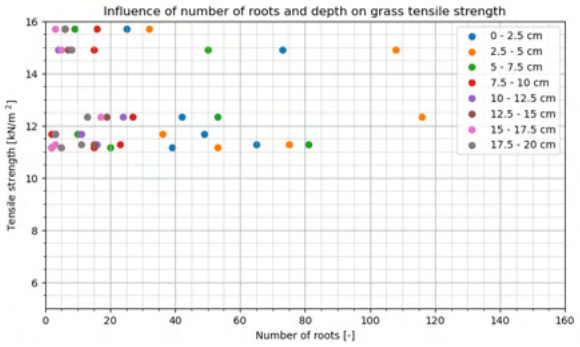

(d) Clay condition 4 submerged

Figure 4.10: Number of roots versus the grass sod strength, plotted for the four normal pull test measurement series.

For this, the measured sod thickness and root length under the sod are plotted for all subconditions in Figure 4.11 and 4.12 respectively. Figure 4.12 shows that for sand, generally longer root lengths are observed than for clay. Also, the variation encountered was larger. During the field measurements, this is also observed. Figure 4.13 shows grass sod samples obtained with the normal pull test.

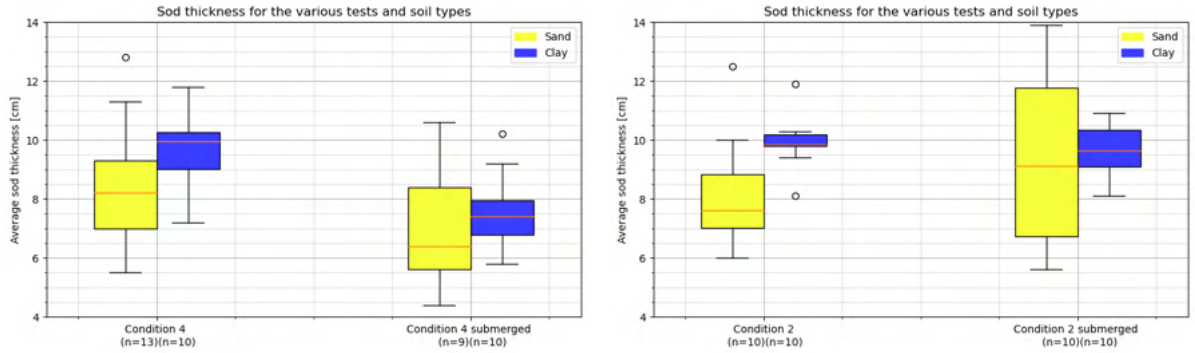

(a) (b)

Figure 4.11: Boxplots displaying the variation of the sod thickness for the normal pull test (a) and for the stepwise increasing constant load test (b).

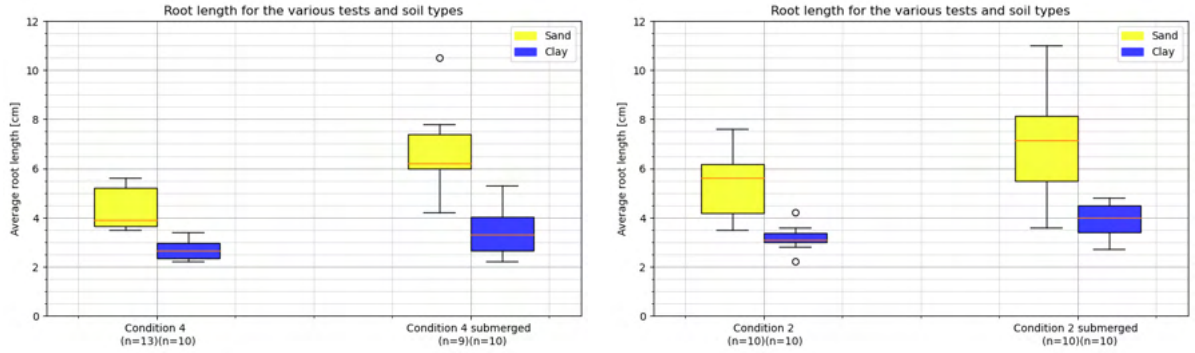

(a) (b)

Figure 4.12: Boxplots displaying the variation of root length for the normal pull test (a) and for the stepwise increasing constant load test (b).

(a) (b)

Figure 4.13: Differences observed for grass sod samples obtained by the normal pull test. (a) shows a grass sod for sand and (b) shows a grass sod for clay. Notice the large irregularity of the failure plane and the long roots for the sandy grass sod. For clay, the failure plane is oriented more or less horizontally while the roots are relatively short. During the experiments, these results were observed most of the time.

When combining the results found in Figure 4.11, 4.12 and 4.13 with the findings for the influences of pore saturation and subsoil type, several conclusions may be drawn for the failure mode of grass covers on sand and on clay. For sandy grass covers, Figure 4.1 showed that the maximum stresses are observed at higher strains than for clayey grass covers. After the maximum stress has been reached, the stress level drops relatively slowly when compared to grass covers on clay, indicating that the sandy grass cover provides ongoing resistance when pulled out. Figure 4.13 shows that the failure plane is irregular, meaning that the sod has a largely variable thickness once it has been pulled out. In the field, the root lengths were found to be shorter for thicker parts and longer for the thinner parts of the sod, which suggests root slip at the thinner parts and root break at the thicker parts of the sod. Concluding, the failure mode for sandy grass covers is suggested to be relatively though and seems to be dominated by both roots slip and root break processes.

For clay, Figure 4.13 shows that the failure plane is approximately horizontal. The roots found at the failure plane are generally short and are less present at larger depth when compared to sandy grass covers, as can be deduced from Figure 4.9. During the normal pull tests, clayey grass covers exhibited a steep rise in stress after an increase in strain. After the maximum measured stress has been reached, a steep drop in stress is observed, indicating that most of the resistance is lost. Hence, failure is relatively instantaneous when compared to sandy grass covers. A possible explanation for this instantaneous failure is that the cohesive clay prevents roots from being pulled out of the soil, preventing root slip processes to determine the strength. As a result, the strength is governed by the magnitude of the cohesion and the root strength. Once the cohesion of the clay is exceeded, a crack develops after which the force is redistributed over the roots. Once the maximum root strength is exceeded, the roots break, leading to failure and a drop of resistance. Cohesive failure and root break seem to coincide as only one stress peak is observed in Figure 4.1, indicating that both processes occur simultaneously. When relating all these observations together, the failure mode of clayey grass covers is expected to be brittle and dominated by the magnitude of the cohesion and the root tensile strength.

When tests are performed during submerged conditions, longer root lengths and thinner sod thicknesses are observed, as can be concluded from Figure 4.12 and 4.13. Strength is generally lower under submerged conditions, as was found in Section 4.1. A possible explanation for these observations may be the reduction of the suction pressures and the decrease of shear forces between the roots and the subsoil as a result of the pore water. This causes the roots to slip rather than to break, leading to longer observed root lengths. Together with the decrease of suction pressures, root slipping processes may contribute to the observed decrease of the grass cover strength during submerged conditions.

To conclude this section, an overview is provided in Table 4.3 showing the main differences found between sandy and clayey grass covers.

Sand	Clay
- Lower resistance to deformation (lower E- and G-modulus) - Still provides resistance after maximum strength - Irregular failure plane - Large variation in root length under sod - Root profile characterised by relatively large number of roots at larger depth - Large spread in pull test results - Lower strength under submerged conditions for normal pull tests	- Higher resistance to deformation (higher E- and G-modulus) - After maximum strength, most resistance is lost - Approximately horizontal failure plane - Small variation in root length under sod - Root profile characterised by low number of roots at larger depth - Relatively small spread in pull test results - Higher strength under submerged conditions for normal pull tests

Table 4.3: Differences observed between sandy and clayey grass covers.

4.3. Influence of fatigue on grass cover strength

4.3.1. Fatigue characteristics

For the fatigue tests, generally three types of results were observed. These are:

1. **Quick failure:** The specimen fails after only a couple of load repetitions.
2. **Delayed failure:** The specimen deforms as the test progresses and ultimately fails after many cycles.
3. **No failure:** The specimen experiences ongoing deformation as the test progresses, however, it does not fail since the test is stopped as a result of the long duration.

Most of the results displayed delayed failure. Grass cover failure during overtopping waves also shows characteristics of delayed failure, as failure is often observed after a significant amount of overtopping waves have passed the grass slope. Hence, the subsequent analyses focus on the fatigue behavior during delayed failure of the grass cover.

Figure 4.14a shows the mean strain development over the course of a fatigue test that displayed delayed failure. The mean strain is calculated by averaging the maximum and minimum strains during a load cycle. A RANSAC-regressor is used to identify the linear part of the graph. For the tests of delayed failure, the three phases in fatigue behavior as mentioned in Section 2.4.4 can clearly be recognized from the graph. The development of the Young's modulus over the course of a fatigue test is displayed in Figure 4.14b. Also for the Young's modulus, the three different phases can be distinguished, starting with a drop in elasticity, followed by stable elasticity decrease and ending with an exponential decrease and ultimately failure.

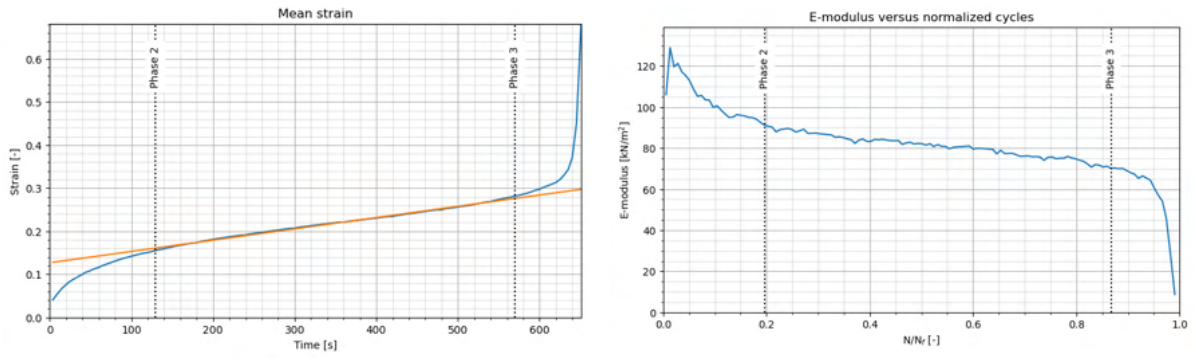

(a) (b)

Figure 4.14: Development of the mean strain (a) and the Young's modulus (b) over the course of a fatigue test.

To investigate the influence of fatigue between the different subsoils, the development of the mean strain and the Young's modulus are plotted in Figure 4.15 and Figure 4.16. The graphs show that the 3 phase behavior is observed for both subsoils. For sand, it seems that initiation of failure can occur at slightly higher strains when

compared to clay. The loss of elasticity is observed to be more severe for a grass cover on clay, as the stiffness decrease is larger than for sand. Since the load has a cyclic nature, it should be noted that the elasticity is based on the differences between the highest and the lowest stresses and strains during a load cycle. As the formulation is different from Equation 3.4 and 3.5, indicative values may deviate with values as determined in Section 4.1.2.

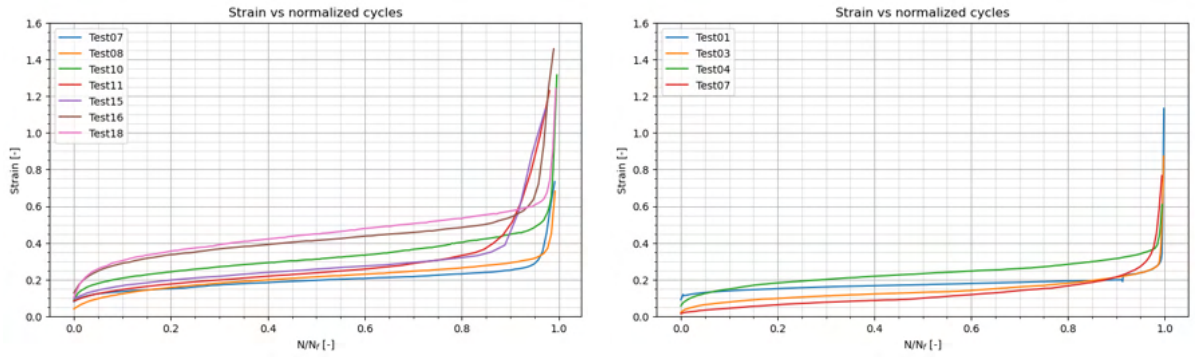

(a) (b)

Figure 4.15: strain development for sand (a) and clay (b). Note that the cycles are normalized.

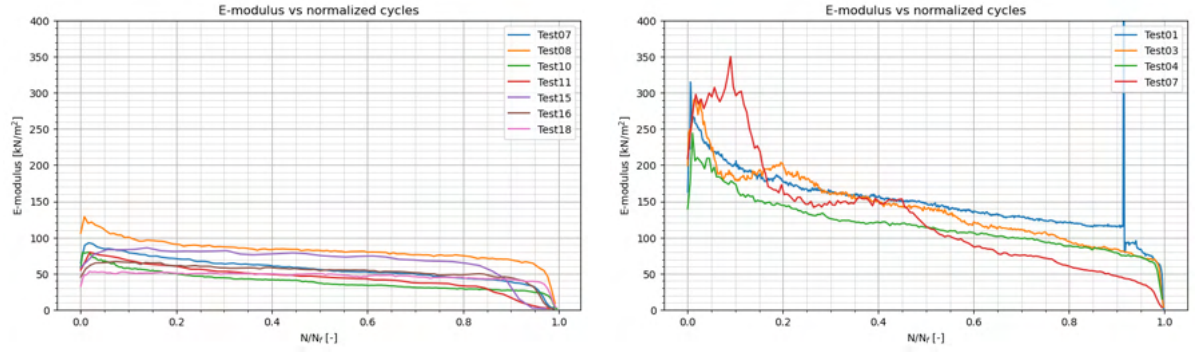

(a) (b)

Figure 4.16: Young's modulus development for sand (a) and clay (b). Note that the cycles are normalized.

4.3.2. Elastic - Plastic behavior

In Figure 4.17, the stress-strain diagram for a fatigue test is displayed. What can be observed from the graph is that the test starts with a relatively large deformation as a result of the induced load. Upon unloading, the material bounces back slightly. However, the material has also deformed permanently and does not return to its original state. In the next cycle, the same happens; the material stretches again as a result of the induced load, bounces back slightly upon unloading, however, also permanent deformation is experienced. As more cycles pass, the permanent deformation of the specimen becomes slightly larger with each cycle, however, the amount by which it does becomes smaller per cycle until an approximately constant permanent deformation growth is reached. This behavior holds until, after many cycles, the loops become horizontally larger while their amplitude decreases; the specimen fails and the strain increases by a large amount. The maximum stress decreases and becomes approximately constant, as a result of the weight of the sample being the only resistance that the pull device experiences.

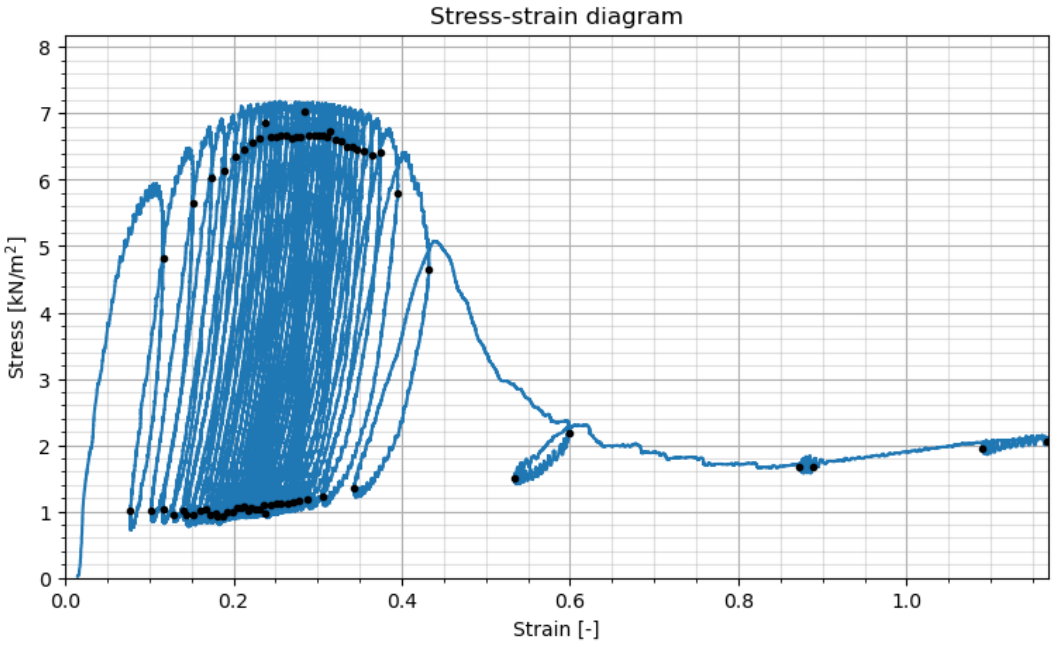

Figure 4.17: Stress-strain diagram for a fatigue test

The 3 phase behavior that is observed may be explained by assuming that the strength of the grass cover is mainly determined by the roots. When the material is intact, the material consists of soil, roots with various diameters and pore water. In the first load cycle, the weakest roots in the grass cover fail easily, after which the load is carried by some stronger roots, which may also fail in the next cycle, etc.. During this first phase, a large plastic deformation growth is observed as a result of these processes. Once the weakest roots have failed, the load is carried by the strongest roots. The roots may have considerable resistance against deformation, which may be determined by their strength or by their interaction with the soil. As a result, the failure of these stronger roots may take considerable time, explaining the slow growth in plastic deformation. Once some of these roots fail, the load is redistributed over the remaining roots. As a larger load is now carried by these roots as a result of the redistribution, failure of these roots is more likely. The process of failure and redistribution of the loads to the ever decreasing number of intact roots explains the quick plastic deformation growth near the failure point.

4.4. Fatigue prediction

4.4.1. S-N curve

The classical way of predicting the design life of a material is by using the S-N curve of the material. In Figure 4.18, the S-N diagram for the performed fatigue tests is displayed, showing the results of the condition 4 submerged fatigue test for both sandy and clayey subsoils. Tests that have been interrupted due to their long duration are included in the plot as runouts.

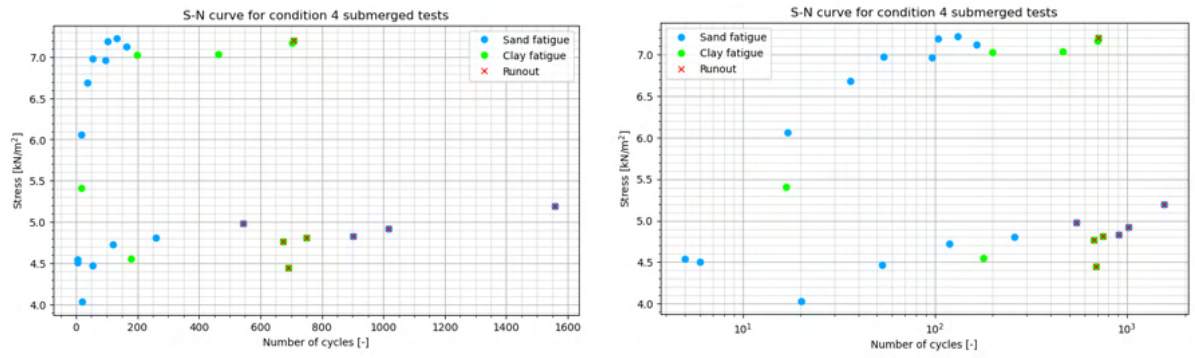

(a) (b)

Figure 4.18: S-N diagrams for the condition 4 submerged fatigue tests. In (a), the cycles are plotted normally and in (b) the cycles are plotted on a log schale.

One of the first things that can be noticed from the plots is the large scatter in results for similar load levels; specimens that are loaded with approximately the same load magnitude either fail after little load repetitions or do not fail at all. Figure 4.18b shows that the duration of the fastest failing test and the longest non-failing test differ by an order of magnitude of approximately three. The spread can be explained by the large variability in material properties, as grass strength is determined by root strength, root-soil interaction, cohesion, suction pressure and other biological properties. These combinations of parameters lead to different fatigue life durations. It should however be noted that a similar order of magnitude is found for the spread of fatigue in other composite materials.

For both soils, fatigue testing was done with two sinusoidally varying load levels, which were chosen at 200 N and 300 N. These can be seen in the plot as two so called data bands, one band at approximately 7 kN/m^2 and one band between 4.5 - 5 kN/m^2. The variation along these bands is caused by the PID-controller, which could not follow the intended load amplitude exactly, but rather approximated it. In fatigue testing, usually more data bands are preferable when constructing a S-N curve, since a better fit may be obtained. The lack of data in combination with the large scatter makes fatigue life prediction by using Figure 4.18 difficult. Other possible prediction methods will be discussed in the following sections.

4.4.2. Absorbed energy

As was observed in Section 4.3.1, the stress-strain diagram for a fatigue test consists of multiple hysteresis loops. Using the stress-strain diagram, one can determine the amount of energy that has dissipated due to deformation of the material, by integrating the area enclosed by a hysteresis loop, as was discussed in Section 2.4.4.

This is done for both soil types in Figure 4.19, which shows the dissipation versus the normalized cycles for the tests that showed 3 phase behavior. Note that the duration of individual tests could vary by a large amount, which is not shown in the graph as a result of the normalization. The figure shows that, most notably for sand, the dissipation per cycle drops at the start of the test, after which the amount of energy dissipation per cycle stays relatively constant. Close to failure, the dissipation increases exponentially as a result of the large deformations. This is reminiscent of the 3 phase fatigue behavior as was found earlier.

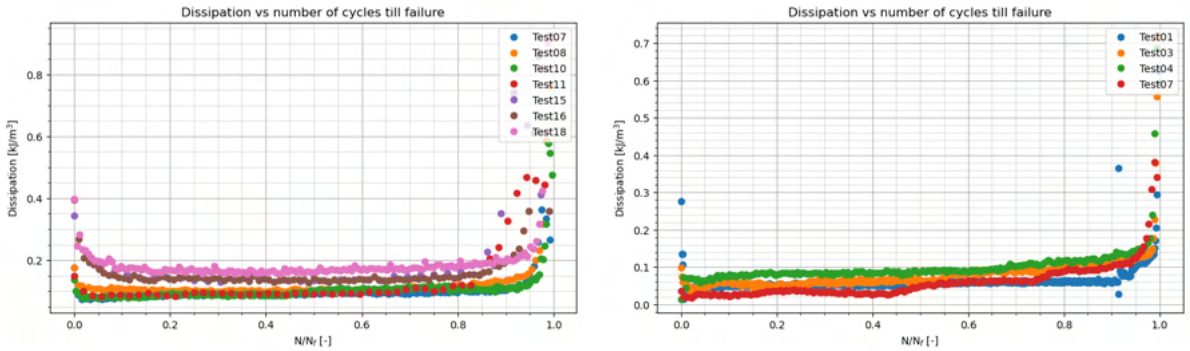

(a) (b)

Figure 4.19: dissipation versus normalized cycles for sand (a) and for clay (b).

An attempt was made to predict the fatigue life with the energy method developed by Stowell (1966), Scott-Emuakpor et al. (2010) and Letcher et al. (2012). For this, it is assumed that the total energy dissipation during a fatigue test is approximately equal to the energy dissipation during a normal pull test. The results showed that predictions for fatigue life were not found to be accurate, as the energy per cycle deviated largely for the various fatigue tests. The spread in the results as observed from Figure 4.18 and Figure 4.18b and the various assumptions that have to be made are expected to be to main reason for not being able to predict the fatigue life.

4.4.3. Strain growth

As could be observed from section 4.3.1, the fatigue behavior of a grass cover displays similar behavior to that of other composite materials, such as concrete. The 3-phase behavior was observed for approximately half of the tested specimen for the condition 4 tests. The other tests were characterised by either very quick failure, which did not yield any 3-phase behavior, or no failure, which made it difficult to judge what phases the sample had ran through. Hence, only the tests that showed clear 3-phase behavior have been used for the strain growth analysis.

Figure 4.20 shows the mean strain development for multiple tests that showed 3-phase behavior, plotted for both a sandy subsoil and a clayey subsoil. As can be observed from the graph, the tests that experienced the fastest growth in strain during phase 2 generally failed the quickest. The strain growth during phase 2 therefore seems to be a good indicator for how quickly a test would fail, although there is still some spread in the results.

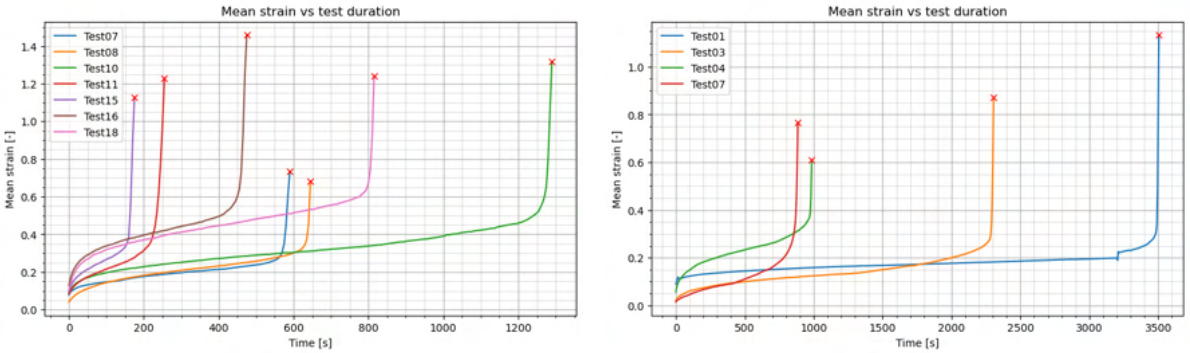

(a) (b)

Figure 4.20: Mean strain versus test duration for sand (a) and for clay (b).

Figure 4.21 shows the slope of the strain during phase 2 versus the number of cycles till failure for tests executed on sandy and clayey subsoils. It can be seen that the function seems to be exponentially decreasing and hence, a lower strain growth leads to a larger number of cycles required for failure to occur. However, as little samples are included in the graph, insight in the actual curve is limited. Construction of a similar graph with the data of future experiments may prove insight into the curve relating fatigue life and strain growth. With a given strain growth found from experiments, the graph may be used to predict the fatigue life of a tested sample.

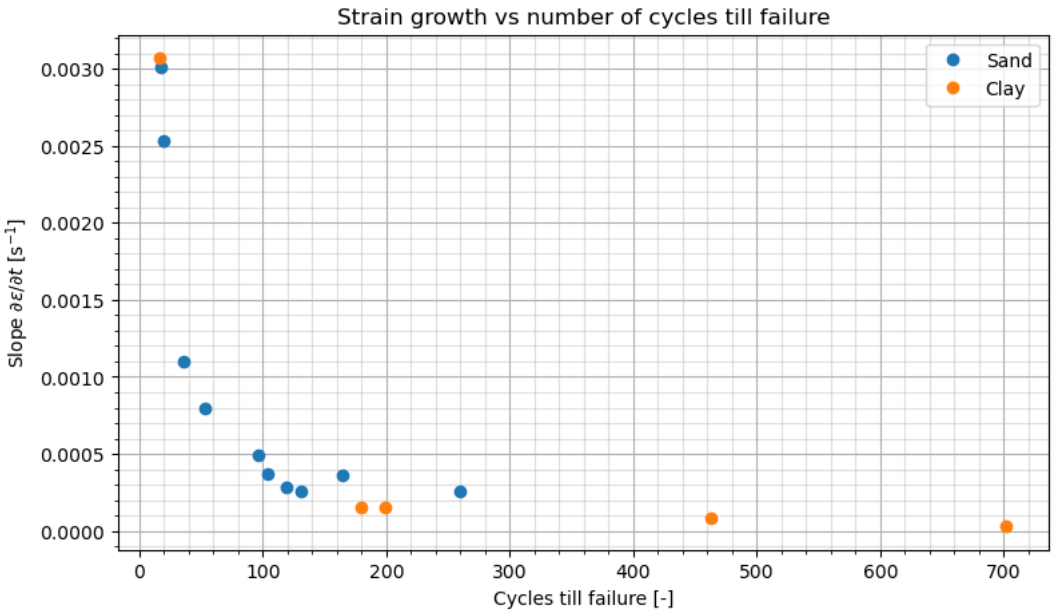

Figure 4.21: Strain growth versus the amount of cycles till failure.

5

Discussion

In this chapter the results from the various field tests are critically reflected upon.Section 5.1 treats the strength analysis and reflects on the calculated Young's and shear moduli for grass covers. Section 5.2 treats the influence of various parameters on the failure plane on the grass cover. The influence of fatigue is treated in Section 5.3. At the end of this chapter, Section 5.4 treats the research limitations and some problems encountered during the execution of the grass pull tests.

5.1. Strength analysis and material properties

5.1.1. Young's modulus and shear modulus

As grass is a composite material, the Young's and shear modulus is determined by a combination of the root, soil and pore water properties. In this section the calculated Young's and shear moduli are validated.

Bijlard (2015) determined Young's moduli using the grass pull test. The assumption was made that only the roots were responsible for the tensile strength. The root area ratio (RAR) that was described in Section 2.4.1 was combined with Equation (3.5) for E_{peak} and yielded mean values of 0.09 GPa. As Bijlard (2015) used a RAR of 0.0008 for good grass covers (Hoffmans et al., 2010), calculation of the composite E-modulus gives an average value of 72 kPa. As Bijlard (2015) did the experiments on a clay dike, average values in this thesis for E_{peak} on clay were found to be twice as large.

Boldrin et al. (2021) calculated tensile stresses and Young's moduli for the roots of various grasses. One of the investigated grasses was perennial ryegrass, a grass which is also found at the Vechtdijk. Values for Young's moduli for the roots of this type of grass were found to be between 21.84 and 74.84 MPa. The formulation which Boldrin et al. (2021) used to calculate E is comparable with Equation (3.4) for $E_{50\%}$. To compare these values, the assumption is made that the tensile strength of the grass cover is entirely caused by the roots. For a sandy subsoil, this may be a valid assumption, since sand is generally not cohesive. When applying the RAR for good grass covers, E-moduli are found between 17.47 and 59.87 kPa, while the results of this thesis show average $E_{50\%}$ values of 89.44 kPa and 73.67 kPa for dry and submerged conditions respectively. Again these values are approximately twice as large compared to the given range of values.

Shear moduli in this thesis were not found to deviate much between sand and clay, while values were found between approximately 8 to 30 kPa. To validate the shear modulus, Equation 2.13 from Section 2.4.2 may be used, which relates the shear modulus to the Young's modulus and the Poisson ratio. Poisson ratio's for sand may range between 0.2 and 0.45, while for clay they may range between 0.3 - 0.45. For sand 0.3 is chosen while for clay 0.4 is chosen. For Young's moduli calculated in this thesis, this yields mean shear moduli of 10.77 kPa for sand and 50.26 kPa for clay. For sand these values are on the low side, while for clay these values are approximately two times as large. When the Young's modulus by Bijlard (2015) is used, shear moduli are found of approximately 26 kPa for both sand and clay. With Young's moduli by Boldrin et al. (2021) a range between 6 kPa and 23 kPa are found, which seem to be the best matching range of values compared to the shear moduli obtained in this thesis.

As elastic moduli were found to differ from literature, seasonal variability of the grass cover may be a possible explanation for the observed differences. Furthermore, various corrections had to be made for calculating the Young's modulus and shear modulus. As mentioned in Section 3.1.4, subsidence played a role during the grass pull test execution. Subsidence is especially important for the calculation of the Young's and shear modulus, since the subsidence correction alters the stress-strain relation. It was found that the corrected values could be up to 85% higher when compared to the uncorrected values, which may explain the observed differences. Although the calculated parameters are found to comply with existing literature, the parameters should be treated with some caution.

Another important aspect to note is that grass cover properties that determine the strength, such as root density and suction pressure, change over the depth. The elastic moduli and shear moduli may therefore be different for different parts of the sod. However, the influence of this is not measured in the field and is therefore outside the scope of this study.

A point to note with regards to the shear modulus is that values are likely overestimated, since two failure planes have been tested. One of the planes is likely to be weaker than the other, and therefore fails earlier. For the determination of the shear modulus, both failure planes have been averaged out.

5.2. Influence of pore saturation, roots and on failure modes

5.2.1. Influence of pore saturation

In general, the grass strength was observed to be negatively influenced by the influence of pore pressure, as was observed for both the submerged normal pull tests as the submerged shear tests. This behavior was also observed during the experiments of Bijlard (2015) and Wegman (2020). As the suction pressure in the grass sod strengthens the grass cover, decrease of the suction pressures as a result of the full saturation may be the cause for the decrease in strength. An additional decrease in strength may also be caused by a larger fraction of roots failing due to slipping as opposed to breaking, as was found by Pollen (2007). From the field tests, it was observed that the grass roots under the sod were generally observed to be longer under submerged conditions, an observation which was also made by Wegman (2020). This implies that more roots stay intact. However, as root length under the sod is a poor measure for estimating how many roots will fail due to slipping and due to breaking and hence, this hypothesis should be verified.

However, not all tests showed a decrease in strength, as several anomalies of this behavior were observed. During submerged normal pull tests for clay, the results showed an increase in strength. Results from grass pull tests by Wegman (2020) also showed this behavior. But also for the submerged shear tests, a third strength peak with a duration of approximately 1 second was observed. A possible hypothesis for these phenomena is that strengthening occurs as a result of under pressures caused by dilatancy of the soil matrix. To investigate whether this hypothesis is true, the time-scale of the phenomenon is investigated. The time-scale in which negative pore pressures diminish is dependant on the hydraulic conductivity and can be estimated with:

$$t = \frac{L}{k} \tag{5.1}$$

In which L is the distance between the location of the under pressure and the atmospheric pressure and k is the hydraulic conductivity of the material. Since grass covers have a structured soil consisting of roots and soil aggregates, the hydraulic conductivity of grass covers is generally larger than for solid clay. Muijs (1999) and Van der Meer et al. (2015) give values of 10^{-4} or 10^{-5} m/s for structured clay opposed to 10^{-9} m/s for solid clay. Since it is assumed that the pores increase slightly as a result of the pull force, the higher conductivity value of 10^{-4} m/s is used for the calculation. With this value a timescale of 1000 seconds for the diminishing of negative pressures is obtained. With this value, it seems unlikely that dilatancy is the cause of the observed strength peaks, as these where only observed during approximately one second. Possible other explanations for the cause of the strength peaks may be the generation of under pressures due to the development of the failure plane or due to the weight of the water on top of the sod providing extra resistance before it flows away. The phenomenon may also have to do with the loading speed of the device, as strengthening was absent for the stepwise increased constant load tests. Further investigations should clarify whether the mentioned hypotheses are true.

5.2.2. Influence of grass roots

As observed in Section 4.2, no correlation was found between the number of roots in the sod and the grass strength. A possible explanation for not finding a correlation may be caused by the way of performing the root counts, on which is elaborated in Section 5.4. Another explanation for the large spread in results is that the strength cannot solely be determined by the number of roots in the sample, but also by other root related parameters such as the root strength. Since roots have multiple diameters, a grass sod with few but large strong roots may be stronger than a grass sod with many but small and weak roots. Additionally, the interaction between roots and soil may cause different failure mechanisms to occur, which may either cause roots being pulled out of the soil or roots breaking (Pollen, 2007). Hence, a densely rooted sod may either fail easily as a result of slip processes or fail with more difficulty due to root break processes. Hence, it may not be strange that such a large spread is observed, as multiple mechanisms are responsible for grass cover failure.

5.2.3. Influence of subsoil

The observations showed that the failure mode for clayey grass covers is different than the failure mode of sandy grass covers. For clayey grass covers the results suggest that most of the roots break, as after the peak strength the clay cover has no resistance left. Furthermore, the failure plane is approximately horizontal and a relatively short root length is observed, which also suggests roots breaking. Cohesion of the clay may be the cause of this failure mode, as it prevents roots from being pulled out of the soil. A similar behavior was observed in the model experiments by Pollen (2007), in which more roots break for soils with higher shear strength.

The observations showed that for a sandy subsoil, the grass cover is easily deformed when loaded. However, after peak strength, the grass cover is still able to provide resistance to the pull force, even at relatively large deformations. This indicates that not all roots fail simultaneously, as opposed to the behavior observed for clayey grass covers. The failure plane is irregular and the root length is relatively long when compared to clay.

5.3. Fatigue tests

The fatigue tests showed a large spread in results that could be distinguished in either quick failure, delayed failure or no failure. In the fatigue tests that showed delayed failure, three different phases could be identified. The three phase fatigue behavior on grass covers was also observed by Wegman (2020). However, since a computer controlled pull device was used opposed to the manually operated pull device used by Wegman (2020), the results in this study provided more clarity on the actual fatigue behavior. The behavior is comparable to the fatigue behavior of other composite materials, such as concrete (Hümme et al., 2016) and fiber-reinforced plastics (Ogin et al., 1985). The finding of the similarity in behavior observed for these materials may lead to several fatigue prediction models to be applicable for grass covers as well.

Quantification of the strength reduction was not revealed in this study, as the test method revealed only insight in the strain and stiffness development over time. As mainly two load levels were tested and a large scatter was observed for the fatigue results, an S-N curve could not be constructed. The scatter in the results for the fatigue life has an order of magnitude of three, a spread that is common in fatigue testing.

5.4. Research Limitations

Although insight into various processes was gained from the experiments, there were several limitations in this research. As was mentioned in Section 2.2, the grass cover properties are found to vary spatially. Additionally, grass cover strength varies largely over time, with the grass being at its weakest during winter and being the strongest during summer. The influence of these spatial and temporal variations falls outside of the scope of this study, although these variations may have influenced the results to a certain extent.

Due to the limited research time, it was chosen to do 10 measurements for each test series to get an idea of the spread in the results. With regards to statistics, this does not have to be the most appropriate sample size to accurately describe the grass cover strength. To get more insight about in how the grass strength is distributed, a larger sample size is advised.

Furthermore, although 180 tests have been performed in total, not all results could be used for the analysis. Occasionally, some unanticipated problems were encountered during the execution of the tests. For some of these tests, this resulted in erroneous test data, which could not be used for further analysis. Some of the most common problems encountered while performing the grass pull tests are treated here as well.

5.4.1. Shear test limitations

The shear test was performed with two sides connected to the grass cover, which caused the development of two failure planes. Hence, the contributions of both sides were measured. Since the weaker failure plane usually fails first, this made it difficult to estimate what the strength of this plane was, since the device measured a single force distributed between the two failure planes. Shear strength and shear modulus values are therefore likely estimated to be too large.

While performing the shear tests, cramps had to be hammered into the ground to fixate the wooden beams. For the tests at the Vechtdijk, the sandy soil was sometimes found to give too little support to these cramps. During testing, the cramps sometimes became loose or got pulled out as a result of the pull force caused by the pull device. This led to some tests not being suitable for analysis, as the sample was not loaded as intended.

For the submerged shear tests, a box had to be installed around the shear test setup to allow the test specimen to be put under water. For the Vechtdijk measurements, this box was found to be not large enough. To install it, it had to cut through the grass at a location close where the wooden beams where installed, creating a failure plane close to the desired failure plane. During test execution, the grass was often found to be failing at this plane instead of the desired failure plane between the wooden beams and the pull frame. Hence, these tests could not be used for data analysis. For the tests at the Waddenzeedijk, two larger boxes were available, which caused no erroneous failure planes during the execution of the tests.

5.4.2. Fatigue test limitations

The fatigue tests have been executed as force-controlled tests, as opposed to the direct pull tests and shear tests, which have been executed as displacement-controlled tests. This was a consequence of the software used to operate the device, which only allowed force-controlled tests to be performed as cyclic tests. As a consequence, the force-controlled tests only provided insight in the displacement of the grass cover. Insight in the strength reduction could not be obtained, as the force was set as a control parameter instead of a measured parameter.

For the stepwise increased constant load tests and the fatigue tests, a PID-controller had to be calibrated to make sure that the desired loading regime would be exerted on the grass cover correctly. The theory of this PID-controller is explained in detail in Appendix C. For some tests, incorrect calibration caused overshooting, which may have influenced the behavior of the test sample over time. Over the course of the measurement campaign, experience was gained with calibration and overshoots were rarely encountered anymore.

From Figure 5.1, it can be noticed that the PID-controller has several implications on the fatigue test. As can be observed, the load is not entirely at it's maximum once the test has started. This is caused by the live calibration of the PID-controller in order to induce the desired load regime on the test sample. The live PID-controller calibration at the start of a test may influence the duration of phase 1, especially for tests that fail relatively quickly.

Another effect caused by the PID-controller is that the load does not reach zero after a cycle, which should be the case. This is also shown in Figure 5.1. This causes some kind of prestressing. In principle, the permanent deformation growth could also be observed when prestressing is present, however, it causes a large initial strain and may therefore influence the duration of phase 1.

Another problem related to the PID-controller was observed as the drop of fatigue load during the fatigue tests. This is illustrated in fig. 5.1. For many of the fatigue tests, the intended load amplitude was found to be decreasing as the tests progressed. This may have been caused by the deformation of the test sample as a result of the varying load, which caused a drop of resistance. Since the PID-controller measures this resisting force in order to control the load, the only way to counter this problem was to readjust the PID-control parameters. Hence, the drop in load was countered by adjusting the PID-control parameters over the course of the test. However, the adjustments may have caused jumpy behavior over the course of some tests, which cannot be attributed to fatigue.

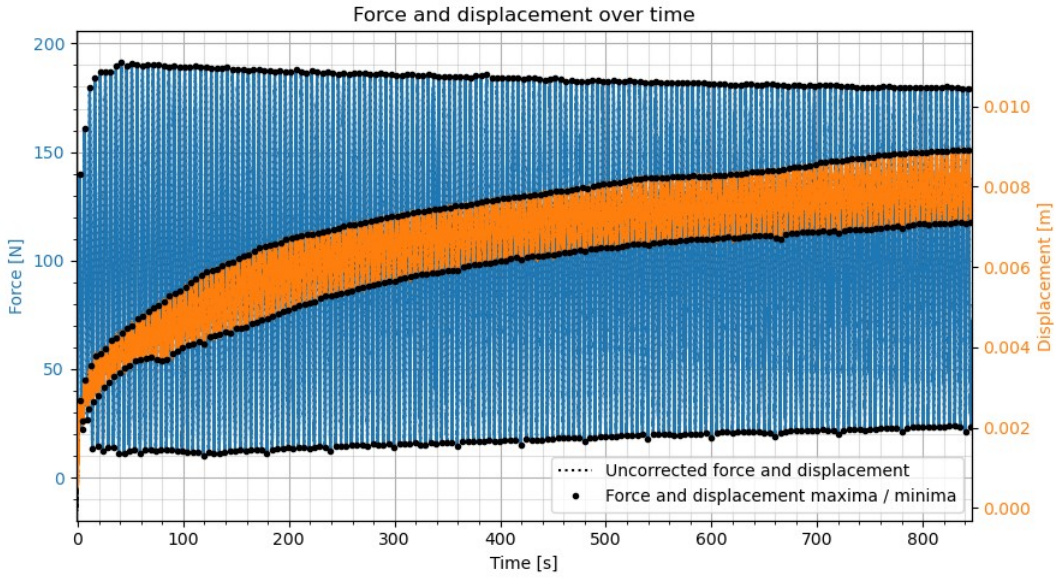

Figure 5.1: Decrease in applied force amplitude (blue) over time

5.4.3. Sod dimensions

To get from measured forces and displacements to stresses and strains, metadata has been recorded containing information about the dimensions and the conditions during testing. Measuring of the sod dimensions was done by means of a yardstick. It should be noted that a grass sod is highly irregular when it has been pulled out by the grass pull device, as can be seen from Figure 3.5. Hence, it was difficult to meausre its exact dimensions. The yardstick is therefore rather used to estimate the dimensions instead of precisely measuring them. This holds mostly for the width and the thickness of the sod.

For the clay dike, it was observed that most grass sods had approximately the same thickness. Further inspection showed a layer of courser gravel stones at the underside of the grass sod. In the excavated parts, sometimes large rubble was found. These things may have influenced the development of the location of the failure plane.

5.4.4. Soil sampling and root counting

Soil sampling is done according to the method described in the VTV2006 report, which is also explained in Section 3.3. With a knife, the sample is subdivided in slices of 2.5 cm thick. A yardstick was used to manually determine the size of the slices. Since this was a manual operation, errors could be easily made. Some slices may be cut too thin or too large, and the roots in the sample made it sometimes difficult to cut the slices. This may have influenced the results obtained for the root counts.

The soil samplings were done after the execution of the pull tests, at a distance of approximately 10 cm from the location of the particular pull test. The aim was to do the sampling as close to the location of the pull test, however, due to the various tests executions some distance had to be taken into account. For instance, when a box was installed for submerged tests, the soil sample was taken away from the box to make sure the sample would not contain roots that may have been damaged by the installation of the box. In hindsight, it would have been better to do the soil sampling before the execution of the pull test. It was found that other parties conducted the soil sampling according to this method.

The root counts have been performed after the measurement campaign was ended. Hence there was a delay of approximately 2 months between soil sampling and root counting. In the meantime, the roots in the samples may have been broken down a bit as a result of biological degradation, which may have resulted in inaccurate counts. However, since there was a large spread encountered in the root profiles, it is difficult to say whether biological degradability took place or may have had an effect on the root counts.

6

Conclusions

For the research objective, it was desired to have a better understanding of the physical processes involved during grass cover failure. The grass pull tests served as the main research method to reach these objectives. This chapter gives the main conclusions for this research and answers the various research questions. To answer the main question:

How can the grass pull device be used to gain insight into the mechanical properties and processes of grass cover failure during wave overtopping?.

With the grass pull test, various experiments have been designed to investigate the influence of several parameters on the grass cover strength. By conducting the grass pull tests as submerged test, the influence of the pore saturation has been investigated. Additionally, by combining the results of grass pull tests with root measurements, the influence of the root reinforcement on the grass cover strength has been tested. By performing experiments on different subsoils, the grass pull device was able to provide insight into the differences between grass covers on sand and on clay. To gain insight into the behavior of the grass cover in the normal direction and shear direction, as well as to gain insight into the material properties Young's and shear modulus, normal pull tests and shear tests could be performed. Furthermore, insight into the progression of damage accumulation is gained by using the grass pull test as a force-controlled fatigue test.

The results in this thesis proved that the grass pull device was able to further improve understanding of the physical characteristics of grass cover failure. Most tests were found to be successful, leading to several new insights regarding failure modes, material properties and fatigue behavior.

How do pore saturation, grass roots and subsoil type influence the failure mode of a grass cover?

In general, the pore saturation was found to be causing lower strength of the grass cover. For both sand and clay, the root lengths were observed to be longer for submerged conditions, which suggests that root slip plays a role in the failure mechanism under submerged conditions.

With regards to the root reinforcement, the results showed that only the number of roots does not solely determine the strength of the grass cover. It is expected that the grass strength depends on other root related properties as well, such as root strength and root interaction with the subsoil. From the measurements of the root length at the underside of the grass sod, it was found that the root lengths for a clay dike are generally shorter than the roots for a sand dike. The failure plane for clay was often found to be oriented more or less horizontally, causing the test sample to have an approximately constant thickness. For sand, the failure plane was found to be irregular, with the thickness varying over the test sample.

Sandy grass covers were found to deform easily. However, the failure mode was found to be relatively tough, providing continuous resistance during deformation. Clayey grass covers provided high resistance against deformation, but showed a quick and brittle failure mode.

What are typical values for the Young's modulus and shear modulus for a grass cover? How is the grass pull test able to quantify these parameters?

With regards to the elastic moduli, values for clay were generally found to lie in the range between 110 kPa and 300 kPa, depending on how the elastic modulus is defined and whether the tests are conducted under submerged conditions or not. For sand, this range is 15 - 130 kPa. The calculated elastic moduli were found to be approximately twice as large as values from literature. Possible causes were explained to be caused by various corrections that had to be made during the analysis of the tests. For this reason, the values should be interpreted with some caution.

Shear moduli between sand and clay are approximately in the same order, with clay having slightly higher values. Obtained Shear modulus values are comparable with literature and are in the range of 8 - 30 kPa. The grass pull test was able to identify these parameters by means of normal pull tests and shear tests.

What is the influence of repeated loading on the tensile strength of a grass cover and how can this effect be quantified?

The measurements have shown that cyclic loading has various effects on the grass cover. From the experiments it was found that the grass cover either fails quickly, delayed or not at all under the effects of repeated loading. The delayed failure mode is the one of interest since it is the failure mode that is often observed during wave overtopping. Similar to other composite materials, such as fiberglass-reinforced polymers that are used in aviation, it is found that grass deformation under cyclic loading is characterised by three phases:

1. Rapid initial deformation during phase one. The growth of the initial deformation stabilizes eventually.
2. Stable, approximately linear deformation growth.
3. Exponentially growing deformation which eventually causes failure after a critical value.

When considering the Young's modulus during fatigue, a similar trend can be observed. The Young's modulus experiences a quick initial drop, after which it decreases approximately linearly. Eventually, the Young's modulus decreases exponentially again until failure.

A quantification of the fatigue strength reduction could not be made, as the fatigue test did not measure the strength reduction. An attempt was made to construct an S-N curve to quantify the strength reduction, however, the large scatter in fatigue results yielded unreliable estimates.

7

Recommendations

The experiments that have been performed in the framework of this thesis has led to several new insights regarding grass cover properties. Based on these results, several recommendations are made to further investigate several aspects that determine the strength of grass covers.

7.1. Device recommendations

The experiments have led to new insights regarding the test device and the experiments itself, and about what tests could be done to further improve the understanding about the strength of grass covers. This section elaborates on several improvements that can be made to further develop the grass pull device.

7.1.1. Submerged pull tests

In this thesis, as well as by results from grass pull tests performed by Wegman (2020), it was found that for quick normal pull tests on clayey subsoils, the strength for grass covers is higher for submerged conditions when compared to dry conditions. For long lasting pull tests such as the stepwise increased constant load tests, this was the opposite, with the strength being lower for submerged conditions when compared to dry conditions. For sandy subsoils, the results for both the quick normal pull tests and the long lasting stepwise increased constant load tests showed also a decrease in strength for submerged conditions.

The cause of this strengthening is unknown, as was discussed in Section 5.2.1. The results of this thesis however shows strange strength peaks for submerged shear tests, for both sandy and clayey subsoils. The strange strength peaks as found during the shear tests may coincide with the strength peak of the normal pull test, causing a higher perceived strength for these tests. As both the normal pull tests and the shear tests are performed as quick tests with a speed of 1 cm/s, the speed of loading may cause these strength peaks to occur. To test whether the phenomenon disappears, the tests can be performed at lower loading speeds. Additionally, the increase of loading speed at the start of the test can be made more gradually, such that the acceleration of the device does not go from zero to 1 cm/s second in a short time span.

7.1.2. Adjusting tripod legs

While preparing the tests, sometimes the pull device could not reach the pull frame. Often the connection could be made when a little force was applied to the top of the pull device. However, this caused prestressing of the grass sod, which affected the obtained results for the Young's and shear modulus. For future measurements, it is therefore advised to make sure the grass pull device could reach the test specimen at all times, to prevent prestressing. Making the legs of the tripod shorter may be a way to solve this issue.

7.1.3. Subsidence correction

The subsidence of the test device caused deviation of the true measured pull force since part of the pull force is absorbed by the ground, causing the subsidence. As a result, the tensile strength and material parameters such as Young's modulus and the shear modulus are likely underestimated. Therefore, either a correction is necessary or the occurring subsidence should be prevented.

Correction may be done by a relatively simple method, such as using ground pegs to measure the subsidence and making the correction. More sophisticated methods can consist of the use of distance sensors to measure the subsidence more accurately. Prevention of subsidence may be achieved by enlarging the tripod feet, such that the pull force is distributed over a larger area, decreasing the load on the soil and causing less subsidence. The question remains if this method causes the force to be reduced enough to prevent subsidence.

7.1.4. Shear tests

The shear tests have been a new way of testing, to identify the contribution of vertical shear to the grass cover strength and to be able to find values for the shear modulus. However, execution of the tests was sometimes cumbersome and therefore it is desired that the method is improved for future experiments.

To make sure the shear test only measures the contribution of one failure plane, a stiff pull frame should be used that is unable to rotate around its axis. Next to this, only one side should be connected to the grass cover, such that only one vertical failure plane develops. In this way, the contributions of the sides can be estimated more accurately and will lead to a better estimate of the strength contribution and the shear modulus.

7.1.5. Fatigue of the grass cover

The results for the fatigue tests have highlighted that the grass cover showed 3-phase behavior when cyclically loaded, which is similar to the behavior of other composite materials during cyclic loading. While the tests have led to these valuable insights, the strength reduction due to fatigue could not be obtained. This is a result of the PID-control mechanism, as fatigue tests have been executed as force controlled tests, with the displacement being the only measured variable. In other areas of engineering such as the aviation industry, fatigue tests are generally performed as displacement controlled tests, with the force being the measured variable. Due to the influence of fatigue, the measured force, or resistance, should decrease over time during these tests.

To gain insight into the strength reduction as a result of fatigue for grass covers, the grass pull tests may be executed as displacement controlled fatigue tests. The result of these tests can be compared with the displacement controlled normal pull tests in order to find the fatigue strength reduction. For the test setup, the displacement amplitude should be chosen carefully; large enough such that failure may occur, however low enough such that immediate rupture is prevented. The results of the fatigue tests that were performed in this thesis, such as the observed displacements and strains, may serve as an input for the design of such experiments.

During execution of the tests using this method some problems might occur. During the fatigue tests, it was observed that the strain keeps increasing as a result of the constant cyclic load. This behavior is likely a result of both root slip and root break processes playing a role in the gradual failure of the grass sod. However, if these tests are performed as displacement controlled tests with a small displacement amplitude, the resisting force decreases as the material deforms. As a result, the ongoing deformation may cause this resisting force to become very small. Hence, the possibility exists that displacement controlled tests will never cause failure. Future field experiments should clarify whether this phenomenon occurs in practice.

7.1.6. Soil sampling and root counts

With the root count measurements performed in this thesis, a distinguishable trend could not be found between the grass tensile strength and the number of roots. The spread in results was explained to also be caused by other root related parameters, such as root strength and root failure mode, which were not included in the assessment. Hence, when only root count measurements are performed, little can be said about the strength of the grass cover. However, root count measurements in combination with for instance strength tests of individual roots may result in a correlation with the tensile tests. Hence, for future research, a strength assessment should be based on a combination of methods to investigate multiple root related parameters, rather than on root count measurements only.

In this thesis, the soil samplings for the root count measurements have been performed at the end of the grass pull tests. Testing was done approximately 10 cm away from the particular grass pull test location. This distance may have resulted in root profiles that describe the actual amount of roots in the grass pull test sample less accurately. For future soil samplings, the sample could be taken significantly closer to the grass pull test sample. It is recommended to take the soil samples before the execution of the pull tests, next to the location where the mold is placed. In this way, the soil samplings do not affect the results for the grass pull tests. The described method was also applied during measurements of third parties.

7.2. Grass pull tests in relation to wave overtopping

The grass pull device has been proven to provide new insights into various processes that occur in the grass cover during failure, as was concluded in Chapter 6. Additionally, from field experiments and from the research by Bijlard (2015), critical velocities from the grass pull test were found to agree reasonably well with critical velocities found from overtopping experiments. Hence, the grass pull test can be used to get an indication of the erosion resistance of the grass cover. However, whether the grass pull device can be used to mimic the loads of overtopping waves and accurately predict the erosion resistance remains questionable. One of the concerns is that the grass pull test is only suitable to simulate pull out erosion, whereas during wave overtopping simulations several other failure modes were found to be responsible for grass cover failure as well, such as wear erosion and jet erosion (Van der Meer et al., 2015). These processes are caused by different load mechanisms, such as the failure initiation process found by Ponsioen (2016).
On a positive note, the grass pull test can be used to get insight into the material parameters and the strength reduction due to fatigue. To do so, either an S-N diagram may be constructed or the load reduction may directly be read from the fatigue tests. In the following sections, a recommendation is made for a method to assess grass cover failure during wave overtopping. The proposed method may serve as a start to relate wave overtopping to grass cover failure.

7.2.1. Methods to determine the hydrodynamic load

To make the connection between the hydrodynamic loads of wave overtopping and the strength of the grass cover, several methods may be used. The validated OpenFOAM® model developed by van Bergeijk et al. (2020) may be used to estimate the pressures, normal stresses and shear stresses acting on the dike. As an alternative, wave overtopping experiments may be executed in which strain gauges or pressure sensors can be used to measure the various shear stresses and pressures acting on the dike.

7.2.2. Method to find the fatigue strength reduction

To find the strength reduction as induced by fatigue, multiple methods can be performed. The first method is the displacement controlled test, which was already described in Section 7.1.5. By performing normal pull tests and displacement controlled fatigue tests, an indication of the strength reduction can already be comparing the results of both tests.

However, to get insight into the fatigue life for different stress levels and the occurrence of a fatigue limit, an S-N diagram should be constructed. To do so, multiple fatigue tests should be performed. The fatigue tests should be executed as submerged tests to mimic the effect of fully saturated conditions, as these conditions usually prevail during wave overtopping tests. Furthermore, the practical method can be used by Bijlard et al. (2016) to determine the strength of the intact grass sod. For this, both condition 2 and condition 4 tests can be performed. A point to note is that the fatigue life may be different for condition 2 and condition 4 tests.

The fatigue tests could either be executed as force controlled tests or displacement controlled tests. What test may be preferable depends on the considerations listed in Section 7.1.5. For the number of tests required, several considerations have to be taken into account. The variability in results of fatigue for composites can differ an order of magnitude of three. Hence, it is desired to do several measurements at the same load level, to get an indication of the variability. Furthermore, fatigue durations are desired for different load levels in order to fit the S-N curve, which requires multiple measurements as well. Hence, a trade off should be made between the desire to gain insight into the variability for constant load levels or the desire to test different load levels. An example of the problem is illustrated in Figure 7.1.

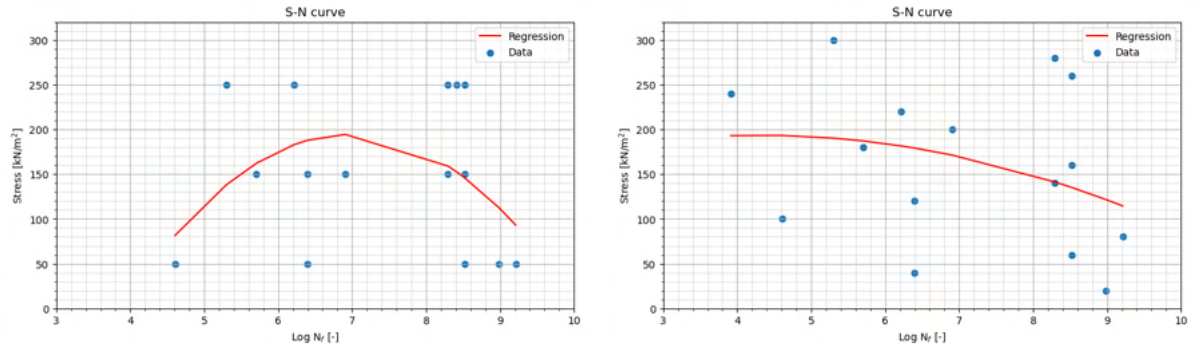

(a) (b)

Figure 7.1: Example of different S-N curves possible using the same number of tests. In (a), each load level is tested five times, showing a variation in fatigue life. The regression shows a strange fit. In (b), the load level of fatigue tests is varied evenly, providing additional information about the variation in stress levels. As a result of the additional information, the regression may show a better fit

Based on these considerations, one fatigue test should be performed per load level. Although a large spread in results may be obtained, information is also provided about the stress distributions, which may lead to a better fit. Figure 7.1 gives an example. The tests should be executed by the top-down approach; The tests with the largest load levels should be executed first, as these often lead to the shortest fatigue life. The load level can be decreased per test in a stepwise manner. Once there is time available for performing additional fatigue tests, these may be performed at the same load levels to increase the confidence of the regression.

Another method that can be used to find a fatigue limit for grass covers is the Staircase method (Schijve, 2001). See Figure 7.2 for an example. For this, the bottom-up approach is used, in which the load level of the fatigue tests are increased with steps until a fatigue test shows failure. The time span N_f in which failure should occur could be chosen, for instance, for grass covers this time can be set as the duration of a storm event. Once a test shows failure, the load level is decreased by one step again and tested if failure occurs within the time span. By doing the tests in this manner, a scatter plot may be obtained, which yields the fatigue limit for the chosen value of N_f.

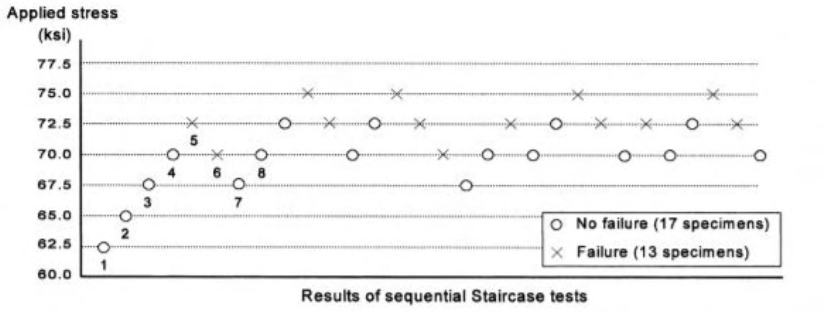

Figure 7.2: Example of the Staircase method for the determination of the fatigue limit. From: Schijve (2001)

For the execution of force controlled fatigue tests, the PID-control mechanism has to be calibrated. More information about calibration of the PID-control mechanism is found in Appendix C. A table with some indicative values for the calibration constants is given in Table 7.1. Note that these are empirically determined constants and they may vary slightly for different grass covers.

Load level	K_p	K_i
100N	-0.01	0.1
200N	-0.015	0.15
300N	-0.025	0.2

Table 7.1: Indicative values for the PID-control mechanism.

Bibliography

Bendoni, M., Georgiou, I., Roelvink, D., and Oumeraci, H. (2019). Numerical modelling of the erosion of marsh boundaries due to wave impact. *Coastal Engineering*, 152:103514.

Bijlard, R. (2015). Strength of the grass sod on dikes during wave overtopping. Report, Delft University of Technology.

Bijlard, R., Steendam, G. J., Verhagen, H. J., and van der Meer, J. (2016). Determining the critical velocity of grass sods for wave overtopping by a grass pulling device. *Coast. Eng. Proc*, 1:20.

Boldrin, D., Bengough, A. G., Lin, Z., and Loades, K. W. (2021). Root age influences failure location in grass species during mechanical testing. *Plant and Soil*, 461(1):457–469.

Cornelissen, H. (1984). Fatigue failure of concrete in tension. *HERON, 29 (4), 1984*.

De Waal, J. P. (2016). Basisrapport wbi 2017. *Versie*, 1:5–73.

Dean, R. G., Rosati, J. D., Walton, T. L., and Edge, B. L. (2010). Erosional equivalences of levees: Steady and intermittent wave overtopping. *Ocean Engineering*, 37(1):104–113.

Hewlett, H., Boorman, L. A., and Bramley, L. (1987). *Design of reinforced grass waterways*. Construction Industry Research and Information Association.

Hoffmans, G., Akkerman, G. J., Verheij, H., van Hoven, A., and Van der Meer, J. (2009). *The erodibility of grassed inner dike slopes against wave overtopping*, pages 3224–3236. World Scientific.

Hoffmans, G., Van Hoven, A., Steendam, G., and Van der Meer, J. (2018). Summary of research work about erodibility of grass revetments on dikes.

Hoffmans, G., van Hoven, A., and Verheij, H. (2010). *Instability of grass caused by wave overtopping*, pages 1023–1032.

Hoffmans, G. J. (2012). *The influence of turbulence on soil erosion*, volume 10. Eburon Uitgeverij BV.

Hughes, S. A. (2011). Adaptation of the levee erosional equivalence method for the hurricane storm damage risk reduction system (hsdrrs). Report, ENGINEER RESEARCH AND DEVELOPMENT CENTER VICKSBURG MS COASTAL AND HYDRAULICS LAB.

Hümme, J., von der Haar, C., Lohaus, L., and Marx, S. (2016). Fatigue behaviour of a normal-strength concrete–number of cycles to failure and strain development. *Structural Concrete*, 17(4):637–645.

Janeček, M., Nový, F., Harcuba, P., Stráský, J., Trško, L., Mhaede, M., and Wagner, L. (2015). The very high cycle fatigue behaviour of ti-6al-4v alloy. *Acta Physica Polonica, A.*, 128(4).

Letcher, T., SHEN, M., Scott-Emuakpor, O., George, T., and Cross, C. (2012). An energy-based critical fatigue life prediction method for al6061-t6. *Fatigue & Fracture of Engineering Materials & Structures*, 35(9):861–870.

Letcher, T., Shen, M.-H. H., Scott-Emuakpor, O., George, T., and Cross, C. (2011). An energy based critical fatigue life prediction method. In *Turbo Expo: Power for Land, Sea, and Air*, volume 54662, pages 77–84.

Mersie, M. (2021). Overtopping failure in levees.

Ministerie van Verkeer en Waterstaat (2007). *Voorschrift toetsen op veiligheid: primaire waterkeringen*. Ministerie van Verkeer en Waterstaat.

Muijs, J. (1999). Grass cover as a dike revetment. *DWW report*.

Ogin, S., Smith, P., and Beaumont, P. (1985). Matrix cracking and stiffness reduction during the fatigue of a (0/90) s gfrp laminate. *Composites Science and Technology*, 22(1):23–31.

Pijpers, R. (2013). Vulnerability of structural transitions in flood defences: erosion of grass covers due to wave overtopping.

Pollen, N. (2007). Temporal and spatial variability in root reinforcement of streambanks: accounting for soil shear strength and moisture. *Catena*, 69(3):197–205.

Ponsioen, L. (2016). Overflow and wave overtopping induced failure processes on the land-side slope of a dike.

Quang, T. T. and Oumeraci, H. (2012). Numerical modelling of wave overtopping-induced erosion of grassed inner sea-dike slopes. *Natural hazards*, 63(2):417–447.

Schijve, J. (2001). *Fatigue of structures and materials*. Springer Science & Business Media.

Schüttrumpf, H. and Oumeraci, H. (2005). Layer thicknesses and velocities of wave overtopping flow at seadikes. *Coastal Engineering*, 52(6):473–495.

Scott-Emuakpor, O., George, T., Cross, C., and Shen, M. H. (2010). Hysteresis-loop representation for strain energy calculation and fatigue assessment. *The Journal of Strain Analysis for Engineering Design*, 45(4):275–282.

Sprangers, J. (1999). *Vegetation dynamics and erosion resistance of sea dyke grassland*.

Steendam, G., De Vries, W., Van der Meer, J., Van Hoven, A., De Raat, G., and Frissel, J. (2009). Influence of management and maintenance on erosive impact of wave overtopping on grass covered slopes of dikes; tests.

Steendam, G. J., Provoost, Y., and Van der Meer, J. (2012). Destructive wave overtopping and wave run-up tests on grass covered slopes of real dikes. *Coastal Engineering Proceedings*, 1(33):structures. 64.

Steendam, G. J., Van Hoven, A., Van der Meer, J., and Hoffmans, G. (2014). Wave overtopping simulator tests on transitions and obstacles at grass covered slopes of dikes. *Coastal Engineering Proceedings*, 1(34):79.

Stowell, E. (1966). A study of the energy criterion for fatigue. *Nuclear Engineering and Design*, 3(1):32–40.

Terzaghi, K. and Peck, R. B. (1948). Soil mechanics in engineering practice.

Valk, A. (2009). Wave overtopping: Impact of water jets on grassed inner slope transitions.

van Bergeijk, V., Warmink, J., Frankena, M., and Hulscher, S. (2019a). Modelling dike cover erosion by overtopping waves: the effects of transitions. *Coastal Structures 2019*, pages 1097–1106.

Van Bergeijk, V., Warmink, J., and Hulscher, S. (2020). Modelling of wave overtopping flow over complex dike geometries: Case study of the afsluitdijk. *Coastal Engineering Proceedings*, (36v):52–52.

Van Bergeijk, V. M. (2018). *The effects of transitions on wave overtopping flow and dike cover erosion for flood defence reliability*. Thesis.

van Bergeijk, V. M., Warmink, J. J., and Hulscher, S. J. (2020). Modelling the wave overtopping flow over the crest and the landward slope of grass-covered flood defences. *Journal of Marine Science and Engineering*, 8(7):489.

van Bergeijk, V. M., Warmink, J. J., van Gent, M. R., and Hulscher, S. J. (2019b). An analytical model of wave overtopping flow velocities on dike crests and landward slopes. *Coastal engineering*, 149:28–38.

van Damme, M. (2016). Distributions for wave overtopping parameters for stress strength analyses on flood embankments. *Coastal Engineering*, 116:195 – 206.

van Damme, M., Ponsioen, L., Herrero Huerta, M., and Peeters, P. (2016). Comparing overflow and wave-overtopping induced breach initiation mechanisms in an embankment breach experiment. *Flood Risk 2016*, 7(03004).

Van der Meer, J. W., Allsop, N. W. H., Bruce, T., De Rouck, J., Kortenhaus, A., Schüttrumpf, H., Troch, P., and Zanuttingh, B. (2018). Eurotop, 2018. manual on wave overtopping of sea defences and related structures. an overtopping manual largely based on european research, but for worldwide application. Report.

Van der Meer, J. W., Bernardini, P., Snijders, W., and Regeling, E. (2007). *The wave overtopping simulator*, pages 4654–4666. World Scientific.

Van der Meer, J. W., Bernardini, P., Steendam, G. J., Akkerman, G. J., and Hoffmans, G. (2009a). *The wave overtopping simulator in action*, pages 645–656. World Scientific.

Van der Meer, J. W., Hardeman, B., Steendam, G. J., Schüttrumpf, H., and Verheij, H. (2010). Flow depths and velocities at crest and landward slope of a dike, in theory and with the wave overtopping simulator. *Coastal Engineering Proceedings*, 1(32):10.

Van der Meer, J. W., Steendam, G. J., De Raat, G., and Bernardini, P. (2009b). *Further developments on the wave overtopping simulator*, pages 2957–2969. World Scientific.

Van der Meer, J. W., van Hoven, A., Paulissen, M., Steendam, G., Verheij, H., Hoffmans, G., and Kruse, G. (2015). Handreiking dijkbekledingen deel 5: Grasbekledingen. Report.

Van Gent, M. R. A. (2002). Low-exceedance wave overtopping events. *Delft Hydraulics project id. DC030202/H3803*.

Van Langevelde, B. (2018). 2d modelling of initiation of failure of a clay slope under wave overtopping load.

Verruijt, A. (2001). *Soil mechanics*. Delft University of Technology Delft.

Wegman, R. J. (2020). Strength of grass covers on dikes. Report.

Winterwerp, J. C. and Van Kesteren, W. G. (2004). *Introduction to the physics of cohesive sediment dynamics in the marine environment*. Elsevier.

Wu, T. H., McKinnell III, W. P., and Swanston, D. N. (1979). Strength of tree roots and landslides on prince of wales island, alaska. *Canadian Geotechnical Journal*, 16(1):19–33.

A

Wave overtopping

In this Appendix, some additional information is given about the mathematical description of wave overtopping. The theory is applied in the design of the wave overtopping simulator and has a strong empirical basis. Run up is discussed in the first section. The second and third section treat overtopping distributions and discharges respectively. Flow velocities and depths are described in the fourth section.

A.0.1. Wave Run-up

Wave overtopping starts with wave run up, which magnitude for gentle slopes is usually defined by the 2% run up height. The EurOtop Manual (Van der Meer et al., 2018) defines the 2% run up height as:

$$\frac{R_{u2\%}}{H_{m0}} = 1.65 \cdot \gamma_b \cdot \gamma_f \cdot \gamma_\beta \cdot \xi_{m-1,0} \tag{A.1}$$

With a maximum of:

$$\frac{R_{u2\%}}{H_{m0}} = 1.0 \cdot \gamma_f \cdot \gamma_\beta \left(4 - \frac{1.5}{\sqrt{\gamma_b \cdot \xi_{m-1,0}}}\right) \tag{A.2}$$

In these relations, $R_{u2\%}$ is the wave run up height that is exceeded by 2% of the waves, H_{m0} the significant wave height and $\xi_{m-1,0}$ is the Irribarren number based on the mean energy wave period $T_{m-1,0}$. γ_b,γ_f and γ_β are correction factors that account for the effects of a berm, the roughness of the slope and the approach angle of the incoming waves respectively.

A.0.2. Overtopping discharges

Overtopping wave discharges are generally expressed in liters per second. The discharges by overtopping waves can be approximated by the following generalized relation (Van der Meer et al., 2018):

$$\frac{q}{\sqrt{g H_{m0}^3}} = a \exp\left[-\left(b \frac{R_c}{H_{m0}}\right)^c\right] \tag{A.3}$$

In which q is the specific discharge, H_{m0} the significant wave height and R_c is the crest freeboard. a,b and c are empirical constants.

A.0.3. Overtopping distributions

For wave overtopping, the amount of overtopping water that flows over the crest is relevant, since overtopping discharge do not give an indication of the amount of water that overtops the dike. Overtopping volumes can be determined by using a Weibull distribution, for which The EurOtop Manual gives:

$$P_V(V_i \geq V) = \exp\left[-\left(\frac{V}{a}\right)\right] \cdot (100\%) \tag{A.4}$$

in which a is a scale factor and b is a shape factor.

A.0.4. Flow velocities and depths

From experiments over the years, many empirical relations have been developed for flow velocities and flow depths over the dike (Schüttrumpf and Oumeraci, 2005; van Bergeijk et al., 2019b; van Damme, 2016; Van der Meer et al., 2018; Van Gent, 2002). The work has been illustrated by Van Bergeijk (2018), who provided a graph comparing the methods derived by Van Gent (2002), Schüttrumpf and Oumeraci (2005) and the EurOtop manual (Van der Meer et al., 2018). The comparison is displayed in Figure A.1.

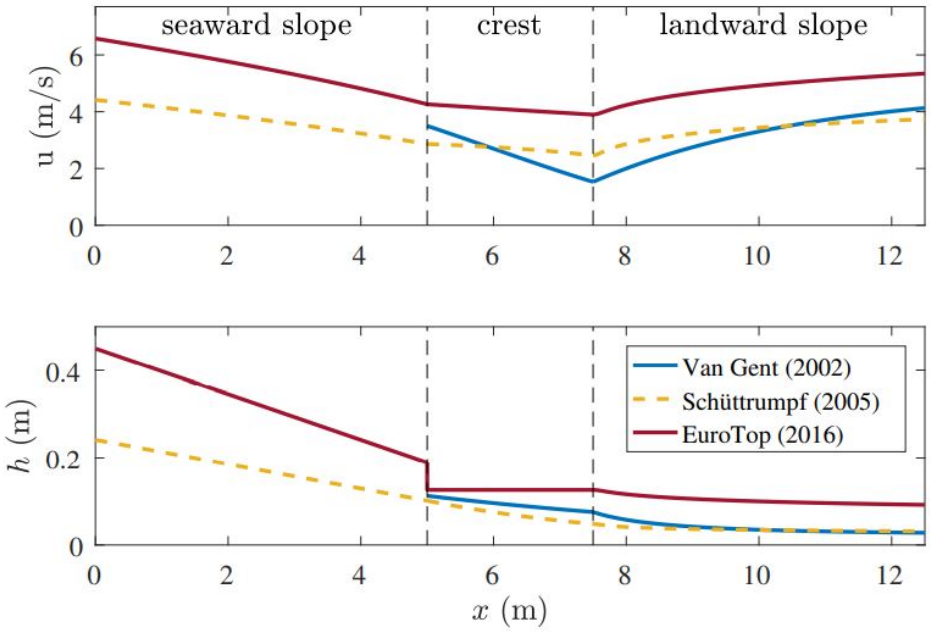

Figure A.1: Flow velocities and depths as determined by multiple studies. The graph shows the development of both parameters for the entire dike profile. From: Van Bergeijk (2018)

The graph shows that at the seaward slope the flow velocity decreases as a result of gravity and friction. At the crest, the flow velocity decreases even further due to friction. At the landward slope, the flow velocity increases again as a result of gravity, but seems to stabilize as the bed friction force will start to balance this gravitational force.

B

Erosion models

This appendix serves as an extension for the theory regarding erosion models, as is described in Section 2.5. The concepts developed by Dean et al. (2010) are treated first, as they serve as a basis for the other models. The widely used Cumulative Overload Method by Van der Meer et al. (2010) is treated second. The Excess Volume Approach by Hughes (2011) is treated third.

B.0.1. Models based on velocity, shear stress and work

Since grass covers are generally eroded gradually instead of instantaneously, the cumulative damaging effect of overtopping waves is of interest when assessing the cover strength. To take this effect into account, Dean et al. (2010) proposed three erosion methods that are based on velocity, shear stress and work respectively. These are given respectively as:

$$E = \sum_{i=1}^{N_c} K(U_i - U_c)\, t_i \tag{B.1}$$

$$E = \sum_{i=1}^{N_c} K(U_i^2 - U_c^2)\, t_i \tag{B.2}$$

$$E = \sum_{i=1}^{N_c} K(U_i^3 - U_c^3)\, t_i \tag{B.3}$$

In which E and K are unknown factors, U_i is the velocity of the incident overtopping wave and t_i is the duration of the overtopping event. U_c again is the threshold velocity above which damage is expected to occur.

To verify the relations, Dean used flow velocities and overtopping durations from laboratory experiments for three different grass cover qualities done by Hewlett et al. (1987). Least squares was used to fit the erosion models. It was found that the work-approach of Equation B.3 provided the best fit for all three grass cover qualities, since for this model the laboratory results had the lowest standard deviation.

B.0.2. Cumulative overload method

Nowadays, the standard approach to assess the strength of a grass cover in the Netherlands is the Cumulative Overload Method, which is developed by Van der Meer et al. (2010). To derive the relation, Van der Meer used the shear stress approach (Equation B.2) as proposed by Dean et al. (2010). Since it was found that damage occurs mostly in the first 1-3 s of the overtopping wave, the time required for each overtopping event was omitted. Based on a damage number, the critical velocity of a grass cover can be determined, which is again the threshold above which damage is expected to occur. The Cumulative Overload Method is given as:

$$D = \sum_{i=1}^{N} \left((U_i)^2 - U_c^2\right) \qquad \text{for} \qquad U_i > U_c \tag{B.4}$$

In which U_i is the front velocity of an incident overtopping wave and U_c is the value for the critical velocity of the grass cover, which is a measure for the grass cover strength. The Cumulative Overload Method is extended over the years with additional factors to account for influences such as change of dike slopes, change of cover

type, obstacles (such as fences or stairs) and acceleration of the overtopping wave running down the slope (Hoffmans et al., 2018). The final result is given by:

$$D = \sum_{i=1}^{N} \left(\alpha_M (\alpha_a U_i)^2 - \alpha_s U_c^2 \right) \qquad \text{for} \qquad \alpha_M (\alpha_a U_i)^2 > \alpha_s U_c^2 \tag{B.5}$$

In this equation, the factor α_a accounts for the increase in flow velocity the overtopping wave experiences while running down the slope as a result of gravity. The factor α_M is a load factor that accounts for the presence of transitions or obstacles. The factor α_s accounts for the strength of the grass at transitions (Hoffmans et al., 2018).

The Cumulative Overload Method has some drawbacks, which has to do with the determination of the damage factor D. While the damage number for failure of the dike is relatively well defined (Steendam et al., 2012), the values for start of damage and damage at multiple locations are not very clear (Hoffmans et al., 2018; Van der Meer et al., 2015).

B.0.3. Excess Volume Approach

Instead of exceeding a critical velocity, Hughes (2011) proposed a relation based on the exceedance of a critical discharge. The damage number in this case is an excess wave volume, which is basically all overtopping wave volumes combined minus the critical volume. The relation is given as:

$$V_E = \int_0^{T_c} q(t) - q_c \, dt \tag{B.6}$$

Using $q = u \cdot h$, the final damage criterion becomes:

$$V_{ET}(t) = \sum_{n=1}^{N_c} V_{Wn} \left[1 - \left(\frac{q_c T_{on}}{V_{Wn}} \right) + \frac{2}{3^{3/2}} \left(\frac{q_c T_{on}}{V_{Wn}} \right)^{3/2} \right] \leq \left(\frac{E_W}{K_W \beta_W} \right) \left(\frac{f_F}{2g \sin\phi} \right) \tag{B.7}$$

With for the critical discharge:

$$q_c = \frac{f_F U_{c,W}^3}{2g \sin\phi} \tag{B.8}$$

In which $V_W n$ and T_{on} are the total volume and the duration of the nth overtopping wave respectively. β_W and f_F are factors accounting for friction.

B.0.4. Application of erosion models

Several models described in this paragraph are being used nowadays in combination with field tests. Especially the Cumulative Overload Method by Van der Meer et al. (2010) is nowadays widely used in combination with the wave overtopping simulator to determine the critical velocity of grass covers.

Bijlard (2015) used Equation 2.24 to determine the critical velocity for a dike slope. For this, a Shields parameter value of 0.03 was assumed. Bijlard made use of the grass pull test in order to find the critical velocity. The results were compared with the critical velocities determined with the overtopping simulator and were found to match quite well. However, it should be noted that the grass pull tests and the overtopping simulator tests have not been done simultaneously. The grass cover characteristics may have varied over time and hence, the results of the comparison have to be approached with some care.

C

PID-controller

For controlling the force or displacement exerted on the grass sod, the grass pull device makes use of a PID-controller. This is a control mechanism that aims at following a specified user input. The PID-controller is used during the stepwise increased constant load tests and the fatigue tests, to make sure the force is exerted on the grass as desired by the user.

The mathematical description for the PID-control mechanism is formulated as:

$$u(t) = K_p e(t) + K_i \int_0^t e(t')\,dt' + K_d \frac{de(t)}{dt} \tag{C.1}$$

With:

$$e(t) = x_{sp} - x(t) \tag{C.2}$$

In these relations, $e(t)$ represents the error between the setpoint x_{sp} and the observed value $x(t)$. For the grass pull device, the setpoint will be provided by the user as a timeseries with setpoint values, whereas the observed value is measured by the device. In this way the error can be calculated at any given time. $u(t)$ is the output parameter, which can either be a force or a displacement in the case of the grass pull device. K_p, K_i and K_d are the respective gain factors. K_p is a factor that converts the error between the setpoint and observed value of the control parameter to the output parameter. The K_i and K_d parameters account for the cumulative effect and the rapid change of the parameter respectively. Since the grass pull device does not make use of the differential part of the PID-controller, the K_d-factor is omitted, or simply set to 0.

C.1. PID-controller calibration

Calibration of the PID-controller is required to make sure that the grass pull device transfers the pull force correctly to the grass cover, in a way that is desired by the user. For the grass pull device, this means that the K_p and K_i control values have to be tweaked. The right combination of K_p and K_i causes the device to follow the user input correctly. However, when the combination is not chosen correctly, the control mechanism may correct too quickly, causing overshoots, or may correct too slowly, causing the setpoints not to be reached, leading to a seemingly damped signal compared to the desired signal. Overshoots are not desired; these may cause the loaded grass cover to fail as a result of the high loading caused by an overshoot. Too much damping is also not desired, since the desired signal will not be followed correctly.

For the grass pull tests, calibration was done in a way to prevent overshooting, since these tests had to be discarded if they would lead to failure. Therefore, calibration was done starting with a combination of K_p and K_i that caused damping, after which these factors where adjusted such that the desired signal was eventually reached. It was found that increasing the K_p factor caused a better direct response, while decreasing the K_i factor caused less damping. The experience of calibrating was gained by performing some trial tests, to get familiar with calibration.